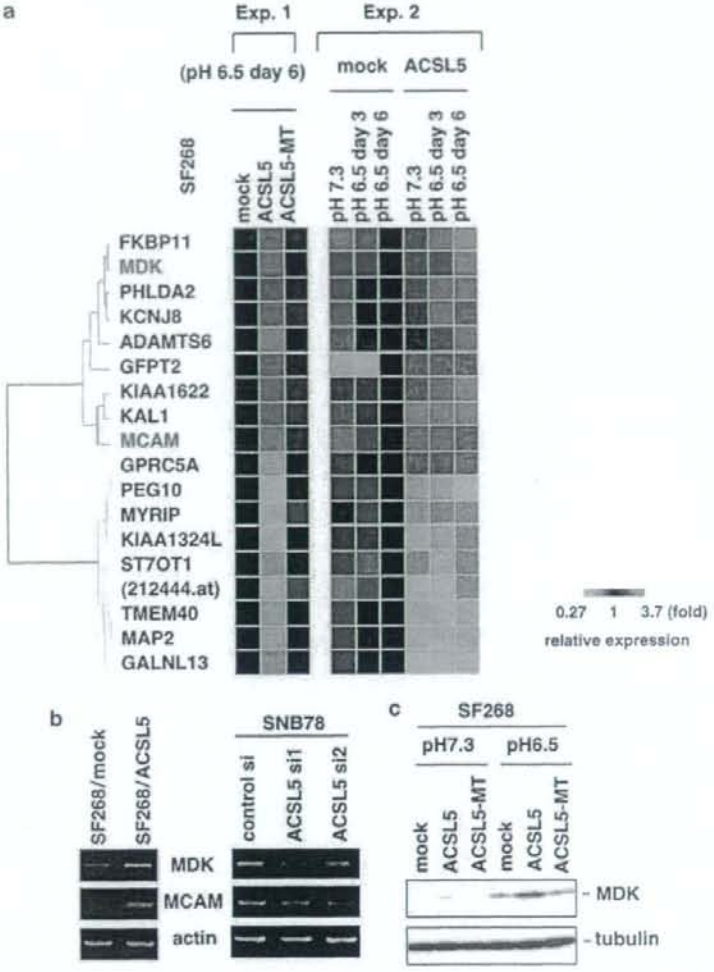


**Figure 4** Identification of acyl-CoA synthetase 5 (ACSL5)-regulated gene expression signature by cDNA microarray analysis. (**a**) Hierarchical clustering using log-transformed relative expression changes over control for genes up- or downregulated exclusively in SF268/ACSL5 cells but not in SF268/ACSL5-MT cells. We applied the arbitrary cutoffs of >2-fold up- or downregulation. Each row and column represents genes and treatment conditions of cells. The values of relative expression changes were calculated over SF268/mock (pH 6.5, day 6) as a baseline. The data in the three left columns and in the six right columns are derived from independent experiments. In each experiment, duplicate samples were analysed. (**b**) ACSL5-dependent regulation of midkine (MDK) and melanoma cell adhesion molecule (MCAM) mRNA expressions. SF268/mock and SF268/ACSL5 cells were cultured for 6 days under acidic conditions (pH 6.5). SNB78 cells were treated with ACSL5 siRNAs or control siRNA and cultured for 48 h under acidic conditions (pH 6.5). Total RNAs were then prepared, and the expressions of MDK and MCAM were analysed by reverse transcription (RT)–PCR. (**c**) ACSL5-dependent regulation of MDK protein expression. SF268/mock, SF268/ACSL5 and SF268/ACSL5-MT cells were cultured for 6 days under normal (pH 7.3) or acidic (pH 6.5) conditions. Cell lysates were prepared, and the expressions of MDK were detected by an anti-MDK antibody. The expressions of α-tubulin were measured as loading controls.

functional ACSL5 is overexpressed in glioma and could have an essential function in glioma cell survival. We have shown earlier that inhibiting multiple ACS activities strongly induces apoptosis, whereas this cell death is almost completely suppressed by a single gene transfer of ACSL5 (Mashima *et al.*, 2005). In addition, among mammalian ACS, only ACSL5 restores the growth of an *Escherichia coli* strain that lacks FadD, the only known ACS enzyme in the *E. coli* (Caviglia *et al.*, 2004). These observations suggest that among ACS members, ACSL5 could have a predominant function in cell survival.

As we have shown, ACSL5 confers selective survival advantage under acidosis conditions but not under other tumor microenvironment stresses. Although we showed that *in vivo* treatment with ACSL5 siRNA significantly suppressed the growth of A1207 tumor (Supplementary Figure 3d), it is still not clear whether

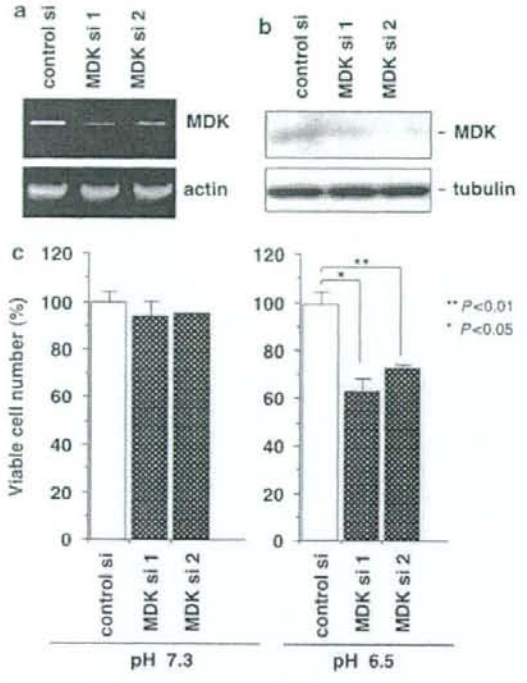


**Figure 5** Involvement of midkine (MDK) in acyl-CoA synthetase 5 (ACSL5)-mediated glioma cell survival under extracellular acidosis conditions. (**a**) mRNA expression of MDK in SF268/ACSL5 cells treated with siRNAs. Cells were treated with stealth siRNAs that targeted MDK, or with control siRNA, as described in Materials and methods. At 48 h after siRNA treatment, total RNAs were prepared and the expressions of MDK were analysed by reverse transcription (RT)–PCR. The expressions of β-actin were also analysed as loading controls. (**b**) Protein expression of MDK in SF268/ACSL5 cells treated with siRNAs. At 48 h after siRNA treatment, cell lysates were prepared and the expressions of MDK were detected by an anti-MDK antibody. The expressions of α-tubulin were also measured as loading controls. (**c**) Viability of SF268/ACSL5 cells after MDK knockdown under normal and acidic conditions. At 24 h after siRNA treatment, SF268/ACSL5 cells were cultured under normal (pH 7.3) or low pH (pH 6.5) conditions for 4 days, and viable cell numbers were counted. Data are mean values of three independent experiments, and error bars show standard deviations. *P*-values (two-sided) were calculated using the Student's *t*-test. *P*-values of $<0.05$ were considered statistically significant. $^{**}P<0.01$; $^{*}P<0.05$.

the expression of ACSL5 alone could be enough to promote tumor growth or survival *in vivo*. To address these questions, we established a tumorigenic U87MG glioma cell line that stably overexpressed ACSL5 and implanted U87MG/mock and U87MG/ACSL5 cells subcutaneously in nude mice. As a result, we did not observe significant advantage of tumor growth in ACSL5-overexpressed U87MG tumors (data not shown). These data suggest that cooperation of ACSL5 with other survival factors could further be required for promotion of glioma growth *in vivo* where several types of stress would coexist.

*Selective induction of MDK gene by ACSL5 under low pH conditions*

Our study showed that ACSL5 is responsible for the expression of some tumor-related factors. Among them, the ACSL5-dependent expression of MDK was critical for survival under acidic conditions. Importantly, the ACSL5-dependent expression of MDK was strongly augmented by low pH stress (Figures 4a and c). This could explain the selective involvement of ACSL5-mediated MDK induction in glioma cell survival under low pH conditions. ACSL5 affects intracellular fatty acid levels through its catalytic activity. These changes may trigger signaling pathways that lead to MDK induction, as fatty acids act as specific ligands for some nuclear receptors, such as peroxisome proliferator-activated receptor (PPAR) (Schoonjans *et al.*, 1996). Although the promoter region of the MDK gene does not possess any direct responsive element for PPAR, it does contain specific elements, including the steroid/thyroid hormone receptor-binding site (TRE) (Uehara *et al.*, 1992). Because PPAR can form a heterodimer with a thyroid hormone receptor (Bogazzi *et al.*, 1994), the element might have a function in the ACSL5-dependent induction of the MDK gene. Our GeneChip microarray analysis revealed that the expression of ACSL5 was not significantly induced under acidic culture conditions (data not shown). These data suggest that although ACSL5 induces the expression of MDK, the acidosis-dependent induction of MDK would be caused by another mechanism.

*Cancer cell survival and growth arrest by MDK*

Several reports have indicated that MDK has a crucial function in the survival and malignant phenotype of cancer (Kadomatsu *et al.*, 1997; Takei *et al.*, 2001; Kadomatsu and Muramatsu, 2004). MDK also confers chemotherapy resistance to cancer cells (Mirkin *et al.*, 2005). Considering the multiple functions of this growth factor, ACSL5-dependent expression of MDK may have a function not only in cell survival under acidosis but also in other malignant phenotypes of cancer cells. Our data indicated that ACSL5 induces MDK expression and concomitantly promotes cell cycle arrest at the G1 phase, especially under extracellular acidosis (Supplementary Figure 2c). It was recently reported that MDK overexpression also promotes cell cycle arrest at the G1 phase (Mirkin *et al.*, 2005). These observations suggest that cell cycle arrest caused by the ACSL5-induced MDK could be important for survival under stress conditions. In fact, G1 arrest is known to be antagonistic to stress-induced cytotoxicity (Knudsen *et al.*, 2000).

*Other factors affected by ACSL5*

We identified MCAM as another factor regulated by ACSL5. Although our data did not show its function in glioma cell survival under low pH, MCAM could have a function in other malignant phenotypes such as tumor metastasis (Xie *et al.*, 1997). Our GeneChip analysis also identified G-protein-coupled receptor C2A (GPRC5A) as a gene selectively downregulated by ACSL5 (Table 1).

GPRC5A was recently reported as a lung tumor suppressor (Tao *et al.*, 2007). In the present analysis, we did not focus on this gene, as its expression was not clearly upregulated in SNB78 cells that were treated with ACSL5 siRNAs (data not shown). Recently, it was shown that ACSL5 partitions exogenously derived fatty acids toward triacylglycerol synthesis and storage (Mashek *et al.*, 2006). The function of this pathway in ACSL5-mediated glioma cell survival should be examined in future studies.

*Global view of the low pH-induced gene expression signature*

We showed that the reduced glioma cell viability under low pH conditions was not derived from caspase-dependent, typical apoptosis (Kitanaka and Kuchino, 1999). Although the mechanisms of the reduced cell viability are still unknown, our analysis identified a set of genes that is highly induced or decreased by low pH stress. These genes included cell death regulators, metastasis suppressors and stress-responsive genes (data not shown). The function of these genes in stress-induced toxicity is still to be clarified.

*Conclusions: ACS as a molecular target for cancer therapy*

Emerging evidence has identified fatty acid metabolisms as promising molecular targets for cancer therapeutics. Among them, ACS members are candidate molecules to induce cancer-selective cell death (Cao *et al.*, 2000; Mashima *et al.*, 2005). Our present data indicate the critical function of ACSL5 in glioma cell survival and suggest that this enzyme could be a rational therapeutic target. On the other hand, our analysis revealed that glioma cells also express other ACS isozymes, including ACSL1, 3 and 4 (data not shown), the functions of which in tumor survival are still unknown. Further analysis including the effect of simultaneous inhibition of multiple ACS isozymes on the survival of cancer could open the door for novel ACS-targeted cancer therapy.

## Materials and methods

*Cell lines, cell culture and measurement of growth inhibition*

Human glioma SF268 and SNB78 cells were cultured in RPMI 1640 supplemented with 10% fetal bovine serum. Human glioma A1207 cells were cultured in Dulbecco's modified Eagle's medium supplemented with 10% fetal bovine serum (Mishima *et al.*, 2001). To examine the effect of extracellular acidosis, the culture medium was acidified by supplementing the regular medium with 25 mM HEPES and adjusting the acidity to a final pH of 6.5 with 0.5 N HCl, as described earlier (Ohtsubo *et al.*, 1997). We measured pH of the medium before and after treatment. Changes in pH were not observed after cells were treated. To estimate the effect of changes in ionic balance and osmolality after the addition of HCl, we added the same concentration (~20 mM) of NaCl to the medium as a control. We found no significant effect of the NaCl addition on glioma cell growth. Hypoxic conditions were achieved using an anaerobic chamber and BBL GasPac Plus (Becton Dickinson, Cockeysville, MD, USA), which catalytically reduces oxygen levels to less than 10 p.p.m. within 90 min (Seimiya *et al.*, 1999). To achieve low serum conditions, we cultured cells in the medium containing 0.1% fetal bovine serum. Cell viability under low pH, hypoxia and low serum or after treatment with siRNA was evaluated by counting viable cells using a hemocytometer. The cell viability was determined by Trypan blue exclusion. Statistical evaluations were performed using Student's *t*-test. *P*-values of $<0.05$ were considered statistically significant.

*Vector construction and retrovirus-mediated gene transfer*

For the expression of human ACSL5, pHa-ACSL5-FLAG-IRES-DHFR was constructed as described earlier (Mashima *et al.*, 2005). To construct an inactive mutant of ACSL5 (ACSL5-MT), we referred to the construction of inactive fatty acid transport protein (FATP1), a very long chain ACSL (Coe *et al.*, 1999). In the case of FATP1, a six-amino-acid substitution into the putative active site (amino acid 249–254: TSGTTG) was enough to inactivate its acyl-CoA synthetase. As ACSL5 also possesses a putative active site with the same sequence (amino acid 261–266: TSGTTG), we converted the amino-acid TSGTT (261–265) to AAAAA to generate pHa-ACSL5-MT-FLAG-IRES-DHFR using a Quik-Change XL site-directed mutagenesis kit (Stratagene, La Jolla, CA, USA). Retrovirus-mediated gene transfer of pHa-IRES-DHFR (mock), pHa-ACSL5-FLAG-IRES-DHFR or pHa-ACSL5-MT-FLAG-IRES-DHFR constructs was performed as described earlier (Mashima *et al.*, 2005).

*siRNA treatment*

siRNA oligonucleotides to ACSL5 were synthesized by Dharmacon Research Inc. (Lafayette, CO, USA). The two siRNAs tested were targeted to the 5′-GCACCAGAGAAGA UAGAAA-3′ (siRNA 1) and 5′-GUGCACUGCUUGUGAG AAA-3′ (siRNA 2) sequences of the human ACSL5 mRNA. As a control, we purchased a nonspecific control duplex (5′-ACUCUAUCUGCACGCUGACUU-3′) from Dharmacon Research Inc. The stealth siRNA oligonucleotides to MDK were synthesized by Invitrogen (Carlsbad, CA, USA). The two siRNAs tested for MDK were 5′-UGAGCAUUGUAGCGC GCCUUCUUCA-3′ (siRNA 1) and 5′-AUUGAUUAAAG CUAACGAGCAGACA-3′ (siRNA 2). A negative universal control siRNA (medium no. 2) was purchased from Invitrogen. siRNAs were transiently introduced into the cells with Lipofectamine 2000 (Invitrogen) according to the manufacturer's instructions.

*Western blot analysis*

Western blot analysis was performed as described earlier (Mashima *et al.*, 2005) with the following primary antibodies: mouse anti-FLAG (M2; Sigma), mouse anti-α-tubulin (Sigma), mouse anti-ACSL5 (Abnova, Taipei, Taiwan) or rabbit anti-MDK (Abcam, Cambridge, UK).

*Measurement of ACS activity*

Total cell lysates were prepared and ACS activity was measured as described earlier (Mashima *et al.*, 2005).

## Acknowledgements

We thank the National Cancer Institute as well as T Yamori for providing us SF268 and SNB78 cell lines and S Aaronson and K Mishima for A1207 cell lines. We thank A Tomida, S Saito and A Furuno for technical advice on GeneChip

analysis, S Okabe for technical support, and T Migita and members in our laboratory for helpful discussions. This study was supported by a Grant-in-Aid for Cancer Research on Priority Areas and a Grant-in-Aid for Young Scientists from the Ministry of Education, Culture, Sports, Science and Technology, Japan.

## References

Bogazzi F, Hudson LD, Nikodem VM. (1994). A novel heterodimerization partner for thyroid hormone receptor. Peroxisome proliferator-activated receptor. *J Biol Chem* **269**: 11683–11686.

Brusselmans K, De Schrijver E, Verhoeven G, Swinnen JV. (2005). RNA interference-mediated silencing of the acetyl-CoA-carboxylase-alpha gene induces growth inhibition and apoptosis of prostate cancer cells. *Cancer Res* **65**: 6719–6725.

Cao Y, Dave KB, Doan TP, Prescott SM. (2001). Fatty acid CoA ligase 4 is up-regulated in colon adenocarcinoma. *Cancer Res* **61**: 8429–8434.

Cao Y, Pearman AT, Zimmerman GA, McIntyre TM, Prescott SM. (2000). Intracellular unesterified arachidonic acid signals apoptosis. *Proc Natl Acad Sci USA* **97**: 11280–11285.

Caviglia JM, Li LO, Wang S, DiRusso CC, Coleman RA, Lewin TM. (2004). Rat long chain acyl-CoA synthetase 5, but not 1, 2, 3, or 4, complements *Escherichia coli* fadD. *J Biol Chem* **279**: 11163–11169.

Coe NR, Smith AJ, Frohnert BI, Watkins PA, Bernlohr DA. (1999). The fatty acid transport protein (FATP1) is a very long chain acyl-CoA synthetase. *J Biol Chem* **274**: 36300–36304.

Coleman RA, Lewin TM, Van Horn CG, Gonzalez-Baro MR. (2002). Do long-chain acyl-CoA synthetases regulate fatty acid entry into synthetic versus degradative pathways? *J Nutr* **132**: 2123–2126.

Gassler N, Herr I, Schneider A, Penzel R, Langbein L, Schirmacher P *et al*. (2005). Impaired expression of acyl-CoA synthetase 5 in sporadic colorectal adenocarcinomas. *J Pathol* **207**: 295–300.

Graeber TG, Osmanian C, Jacks T, Housman DE, Koch CJ, Lowe SW *et al*. (1996). Hypoxia-mediated selection of cells with diminished apoptotic potential in solid tumours. *Nature* **379**: 88–91.

Harris AL. (2002). Hypoxia—a key regulatory factor in tumour growth. *Nat Rev Cancer* **2**: 38–47.

Hatzivassiliou G, Zhao F, Bauer DE, Andreadis C, Shaw AN, Dhanak D *et al*. (2005). ATP citrate lyase inhibition can suppress tumor cell growth. *Cancer Cell* **8**: 311–321.

Ikematsu S, Yano A, Aridome K, Kikuchi M, Kumai H, Nagano H *et al*. (2000). Serum midkine levels are increased in patients with various types of carcinomas. *Br J Cancer* **83**: 701–706.

Jia HL, Ye QH, Qin LX, Budhu A, Forgues M, Chen Y *et al*. (2007). Gene expression profiling reveals potential biomarkers of human hepatocellular carcinoma. *Clin Cancer Res* **13**: 1133–1139.

Kadomatsu K, Hagihara M, Akhter S, Fan QW, Muramatsu H, Muramatsu T. (1997). Midkine induces the transformation of NIH3T3 cells. *Br J Cancer* **75**: 354–359.

Kadomatsu K, Muramatsu T. (2004). Midkine and pleiotrophin in neural development and cancer. *Cancer Lett* **204**: 1391–1399.

Kitanaka C, Kuchino Y. (1999). Caspase-independent programmed cell death with necrotic morphology. *Cell Death Differ* **6**: 508–515.

Knudsen KE, Booth D, Naderi S, Sever-Chroneos Z, Fribourg AF, Hunton IC *et al*. (2000). RB-dependent S-phase response to DNA damage. *Mol Cell Biol* **20**: 7751–7763.

Kuhajda FP. (2006). Fatty acid synthase and cancer: new application of an old pathway. *Cancer Res* **66**: 5977–5980.

Lewin TM, Kim JH, Granger DA, Vance JE, Coleman RA. (2001). Acyl-CoA synthetase isoforms 1, 4, and 5 are present in different subcellular membranes in rat liver and can be inhibited independently. *J Biol Chem* **276**: 24674–24679.

Liang YC, Wu CH, Chu JS, Wang CK, Hung LF, Wang YJ *et al*. (2005). Involvement of fatty acid-CoA ligase 4 in hepatocellular carcinoma growth: roles of cyclic AMP and p38 mitogen-activated protein kinase. *World J Gastroenterol* **11**: 2557–2563.

Maeda S, Shinchi H, Kurahara H, Mataki Y, Noma H, Maemura K *et al*. (2007). Clinical significance of midkine expression in pancreatic head carcinoma. *Br J Cancer* **97**: 405–411.

Mashek DG, McKenzie MA, Van Horn CG, Coleman RA. (2006). Rat long chain acyl-CoA synthetase 5 increases fatty acid uptake and partitioning to cellular triacylglycerol in McArdle-RH7777 cells. *J Biol Chem* **281**: 945–950.

Mashima T, Oh-hara T, Sato S, Mochizuki M, Sugimoto Y, Yamazaki K *et al*. (2005). p53-defective tumors with a functional apoptosome-mediated pathway: a new therapeutic target. *J Natl Cancer Inst* **97**: 765–777.

Mashima T, Tsuruo T. (2005). Defects of the apoptotic pathway as therapeutic target against cancer. *Drug Resist Updat* **8**: 339–343.

Menendez JA, Lupu R. (2007). Fatty acid synthase and the lipogenic phenotype in cancer pathogenesis. *Nat Rev Cancer* **7**: 763–777.

Mirkin BL, Clark S, Zheng X, Chu F, White BD, Greene M *et al*. (2005). Identification of midkine as a mediator for intercellular transfer of drug resistance. *Oncogene* **24**: 4965–4974.

Mishima K, Asai A, Kadomatsu K, Ino Y, Nomura K, Narita Y *et al*. (1997). Increased expression of midkine during the progression of human astrocytomas. *Neurosci Lett* **233**: 29–32.

Mishima K, Johns TG, Luwor RB, Scott AM, Stockert E, Jungbluth AA *et al*. (2001). Growth suppression of intracranial xenografted glioblastomas overexpressing mutant epidermal growth factor receptors by systemic administration of monoclonal antibody (mAb) 806, a novel monoclonal antibody directed to the receptor. *Cancer Res* **61**: 5349–5354.

Nakagawara A, Milbrandt J, Muramatsu T, Deuel TF, Zhao H, Cnaan A *et al*. (1995). Differential expression of pleiotrophin and midkine in advanced neuroblastomas. *Cancer Res* **55**: 1792–1797.

O'Brien T, Cranston D, Fuggle S, Bicknell R, Harris AL. (1996). The angiogenic factor midkine is expressed in bladder cancer, and overexpression correlates with a poor outcome in patients with invasive cancers. *Cancer Res* **56**: 2515–2518.

Ohtsubo T, Wang X, Takahashi A, Ohnishi K, Saito H, Song CW *et al*. (1997). p53-dependent induction of WAF1 by a low-pH culture condition in human glioblastoma cells. *Cancer Res* **57**: 3910–3913.

Reichert M, Steinbach JP, Supra P, Weller M. (2002). Modulation of growth and radiochemosensitivity of human malignant glioma cells by acidosis. *Cancer* **95**: 1113–1119.

Rofstad EK, Mathiesen B, Kindem K, Galappathi K. (2006). Acidic extracellular pH promotes experimental metastasis of human melanoma cells in athymic nude mice. *Cancer Res* **66**: 6699–6707.

Schoonjans K, Staels B, Auwerx J. (1996). Role of the peroxisome proliferator-activated receptor (PPAR) in mediating the effects of fibrates and fatty acids on gene expression. *J Lipid Res* **37**: 907–925.

Seimiya H, Tanji M, Oh-hara T, Tomida A, Naasani I, Tsuruo T. (1999). Hypoxia up-regulates telomerase activity via mitogen-activated protein kinase signaling in human solid tumor cells. *Biochem Biophys Res Commun* **260**: 365–370.

Soengas MS, Alarcon RM, Yoshida H, Giaccia AJ, Hakem R, Mak TW *et al*. (1999). Apaf-1 and caspase-9 in p53-dependent apoptosis and tumor inhibition. *Science* **284**: 156–159.

Sung YK, Hwang SY, Park MK, Bae HI, Kim WH, Kim JC *et al*. (2003). Fatty acid-CoA ligase 4 is overexpressed in human hepatocellular carcinoma. *Cancer Sci* **94**: 421–424.

Sung YK, Park MK, Hong SH, Hwang SY, Kwack MH, Kim JC *et al*. (2007). Regulation of cell growth by fatty acid-CoA ligase 4 in human hepatocellular carcinoma cells. *Exp Mol Med* **39**: 477–482.

Takei Y, Kadomatsu K, Matsuo S, Itoh H, Nakazawa K, Kubota S *et al*. (2001). Antisense oligodeoxynucleotide targeted to Midkine, a heparin-binding growth factor, suppresses tumorigenicity of mouse rectal carcinoma cells. *Cancer Res* **61**: 8486–8491.

Tannock IF, Rotin D. (1989). Acid pH in tumors and its potential for therapeutic exploitation. *Cancer Res* **49**: 4373–4384.

Tao Q, Fujimoto J, Men T, Ye X, Deng J, Lacroix L *et al*. (2007). Identification of the retinoic acid-inducible Gprc5a as a new lung tumor suppressor gene. *J Natl Cancer Inst* **99**: 1668–1682.

Tomida A, Tsuruo T. (1999). Drug resistance mediated by cellular stress response to the microenvironment of solid tumors. *Anticancer Drug Des* **14**: 169–177.

Tong Y, Mentlein R, Buhl R, Hugo HH, Krause J, Mehdorn HM *et al.* (2007). Overexpression of midkine contributes to anti-apoptotic effects in human meningiomas. *J Neurochem* **100**: 1097–1107.

Uehara K, Matsubara S, Kadomatsu K, Tsutsui J, Muramatsu T. (1992). Genomic structure of human midkine (MK), a retinoic acid-responsive growth/differentiation factor. *J Biochem* **111**: 563–567.

van den Beucken T, Koritzinsky M, Wouters BG. (2006). Translational control of gene expression during hypoxia. *Cancer Biol Ther* **5**: 749–755.

Vaupel P, Kallinowski F, Okunieff P. (1989). Blood flow, oxygen and nutrient supply, and metabolic microenvironment of human tumors: a review. *Cancer Res* **49**: 6449–6465.

Xie S, Luca M, Huang S, Gutman M, Reich R, Johnson JP *et al.* (1997). Expression of MCAM/MUC18 by human melanoma cells leads to increased tumor growth and metastasis. *Cancer Res* **57**: 2295–2303.

Yamashita Y, Kumabe T, Cho YY, Watanabe M, Kawagishi J, Yoshimoto T *et al.* (2000). Fatty acid induced glioma cell growth is mediated by the acyl-CoA synthetase 5 gene located on chromosome 10q25.1–q25.2, a region frequently deleted in malignant gliomas. *Oncogene* **19**: 5919–5925.

Ye C, Qi M, Fan QW, Ito K, Akiyama S, Kasai Y *et al.* (1999). Expression of midkine in the early stage of carcinogenesis in human colorectal cancer. *Br J Cancer* **79**: 179–184.

Yeh CS, Wang JY, Cheng TL, Juan CH, Wu CH, Lin SR. (2006). Fatty acid metabolism pathway play an important role in carcinogenesis of human colorectal cancers by microarray-bioinformatics analysis. *Cancer Lett* **233**: 297–308.

Supplementary Information accompanies the paper on the Oncogene website (http://www.nature.com/onc)

Oncogene (2008) 27, 1677–1686

www.nature.com/onc

ORIGINAL ARTICLE

# FOXO transcription factor-dependent p15$^{INK4b}$ and p19$^{INK4d}$ expression

K Katayama[1,2], A Nakamura[1,3], Y Sugimoto[1,2], T Tsuruo[1] and N Fujita[1]

[1]*Cancer Chemotherapy Center, Japanese Foundation for Cancer Research, Tokyo, Japan;* [2]*Department of Chemotherapy, Kyoritsu University of Pharmacy, Tokyo, Japan and* [3]*Institute of Molecular and Cellular Biosciences, The University of Tokyo, Tokyo, Japan*

**FOXO (Forkhead box O) transcription factors are involved in cell-cycle arrest or apoptosis induction by transcripting cell-cycle inhibitor $p27^{KIP1}$ or apoptosis-related genes, respectively. Akt/protein kinase B promotes cell proliferation and suppresses apoptosis, in part, by phosphorylating FOXOs. Phosphorylated FOXOs could not exhibit transcriptional activity because of their nuclear export. Here we show that $p15^{INK4b}$ and $p19^{INK4d}$ transcription is associated with FOXO-mediated $G_1$ cell-cycle arrest. Inhibition of Akt signaling by PI3K inhibitors, a PDK1 inhibitor, or dominant-negative Akt transfection increased expression of p15$^{INK4b}$ and p19$^{INK4d}$ but not p16$^{INK4a}$ and p18$^{INK4c}$. Ectopic expression of wild type or active FOXO but not inactive form also increased p15$^{INK4b}$ and p19$^{INK4d}$ levels. FOXOs bound to promoter regions and induced transcription of these genes. No increase in the $G_1$-arrested cell population, mediated by PI3K inhibitor LY294002, was observed in $INK4b^{-/-}$ or $INK4d^{-/-}$ murine embryonic fibroblasts. In summary, FOXOs are involved in $G_1$ arrest caused by Akt inactivation via $p15^{INK4b}$ and $p19^{INK4d}$ transcription.**

*Oncogene* (2008) **27**, 1677–1686; doi:10.1038/sj.onc.1210813; published online 17 September 2007

**Keywords:** Akt; FOXO; INK4

## Introduction

Akt (also known as protein kinase B, PKB) signaling pathway controls many cellular functions, such as cell survival, cell-cycle progression, cell proliferation, apoptosis inhibition, protein synthesis and glucose metabolism (Matsushima-Nishiu *et al.*, 2001; Tsuruo *et al.*, 2003; Katayama *et al.*, 2005). A large number of cancers are known to aberrantly activate this pathway, resulting in cancer cell survival and proliferation. Activation of this pathway normally depends on growth factor stimulation. Growth factors activate phosphatidylinositide-3-OH kinase (PI3K) and then lead to recruitment of 3-phosphoinositide-dependent protein kinase 1 (PDK1) and Akt on the plasma membrane (Vanhaesebroeck and Alessi, 2000; Tsuruo *et al.*, 2003). PDK1 and other kinases convert Akt from an inactive form to an active form by phosphorylation.

FOXO (named for the Forkhead box O) transcription factors, such as FOXO1a, FOXO3a and FOXO4 (also known as FKHR, FKHRL1 and AFX, respectively), were identified at chromosomal breakpoints in human tumors (Woods and Rena, 2002). FOXOs are direct targets of Akt phosphorylation and are negatively regulated by Akt (Brunet *et al.*, 1999; Woods and Rena, 2002). Akt-dependent phosphorylation of FOXOs results in their cytoplasmic localization, possibly by association with 14-3-3 proteins, and inability to exhibit their gene transcriptional activity (Brunet *et al.*, 1999; Woods and Rena, 2002). FOXOs are reported to be involved in apoptosis induction or cell-cycle arrest by transcription of the related genes (Medema *et al.*, 2000; Rokudai *et al.*, 2002; Stahl *et al.*, 2002; Suhara *et al.*, 2002).

Eukaryotic cell-cycle progression is strictly regulated and promoted by the activity of phase-specific kinase complexes composed of cyclin and cyclin-dependent kinase (CDK). Cyclin D–CDK4/6 complexes promote middle $G_1$ phase and then cyclin E–CDK2 complex promotes late $G_1$ phase. CDK inhibitors (CKIs) consist of INK4 and CIP/KIP families and induce cell-cycle arrest by blocking the activity of cyclin–CDK complexes (Sherr and Roberts, 1995; LaBaer *et al.*, 1997). The INK4 family (p16$^{INK4a}$, p15$^{INK4b}$, p18$^{INK4c}$ and p19$^{INK4d}$) specifically binds to and inhibits cyclin D–CDK4/6 complexes, while the CIP/KIP family (p21$^{CIP1}$, p27$^{KIP1}$ and p57$^{KIP2}$) binds to and inhibits the cyclin E–CDK2 complex as well as other cyclin–CDK complexes operating throughout the cell cycle. In quiescent cells, CKIs are present in excess to cyclin–CDK complexes, so the cells are maintained in a non-proliferating state. CKIs are therefore critical mediators of antiproliferative signals, cell-cycle arrest, DNA repair, terminal differentiation and senescence.

The tumor suppressor gene product phosphatase and tensin homologue deleted on chromosome 10 (PTEN) is a lipid phosphatase. PTEN antagonizes PI3K function and prevents PDK1 and Akt from recruiting to the plasma membrane, resulting in inactivation of Akt signaling pathway. Adenoviral transduction of PTEN into PTEN-defective HEC-151 cells was reported to promote $p15^{INK4b}$ mRNA expression in DNA microarray and reverse transcription (RT)–PCR analyses (Matsushima-Nishiu

Correspondence: Dr N Fujita, Division of Experimental Chemotherapy, Cancer Chemotherapy Center, Japanese Foundation for Cancer Research, Tokyo 135-8550, Japan.
E-mail: naoya.fujita@jfcr.or.jp
Received 11 May 2007; revised 15 August 2007; accepted 23 August 2007; published online 17 September 2007

*et al.*, 2001). However, it is unknown whether p15$^{INK4b}$ protein is actually involved in the $G_1$ arrest and how the Akt signaling pathway regulates p15$^{INK4b}$ expression. In this study, we show that FOXO transcription factors transcript not only *p15$^{INK4b}$* but also *p19$^{INK4d}$* genes. Furthermore, the PI3K inhibitor LY294002 failed to cause $G_1$ arrest in *p15$^{INK4b}$*- or *p19$^{INK4}$*-null mouse-derived embryonic fibroblasts (*INK4b$^{-/-}$* or *INK4d$^{-/-}$* murine embryonic fibroblasts (MEFs)). Thus, FOXO-mediated *p15$^{INK4b}$* and *p19$^{INK4d}$* transcription is involved in $G_1$ cell-cycle arrest caused by Akt inhibition.

## Results

### *Akt inhibition causes $G_1$ arrest by upregulating p15$^{INK4b}$ and p19$^{INK4d}$ expression*

To clarify the regulation of INK4 family protein expression by the Akt signaling, we first examined the change of INK4-family protein expression before and after treatment of 293T cells with the PI3K inhibitor Wortmannin or the PDK1 inhibitor Celecoxib for 24 h. Consistent with the previous reports (Sherr and Roberts, 1995; Medema *et al.*, 2000), inhibition of Akt signaling upregulated p27$^{KIP1}$ expression (Figure 1a). Further, we observed a drastic increase in p15$^{INK4b}$ and p19$^{INK4d}$ protein, while inhibition of Akt signaling showed no effect on p16$^{INK4a}$ and p18$^{INK4c}$ protein levels (Figure 1a). To confirm these findings, we treated 293T, HepG2 and Raji cells with another PI3K inhibitor LY294002 for 24 h. Western blot and RT–PCR analyses clearly indicated that PI3K inhibition by LY294002 caused p15$^{INK4b}$ and p19$^{INK4d}$ protein and mRNA expressions in each cell line (Figures 1b and c). The p16$^{INK4a}$ and p18$^{INK4c}$ expression levels were not affected by LY294002 treatment.

Because INK4 family proteins specifically bound to and inhibited cyclin D–CDK4/6 complexes, inhibition of Akt signaling pathway might cause cell-cycle arrest. We confirmed CDK4 and CDK6 kinase activities before and after treatment of 293T cells with LY294002.

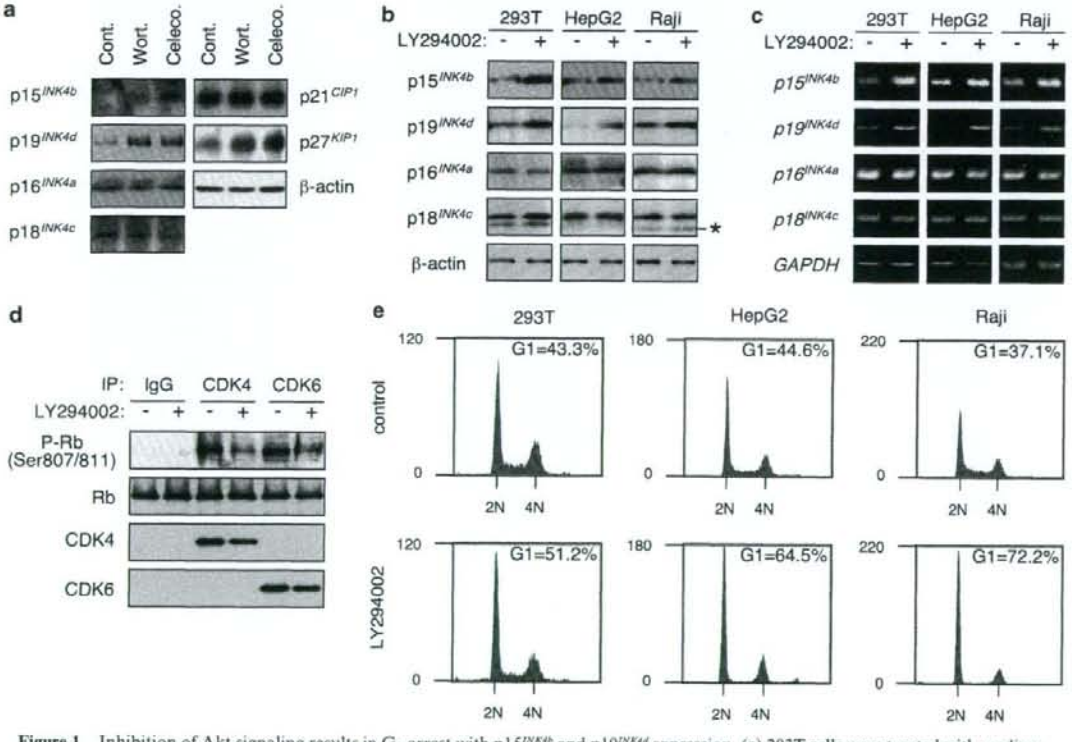


**Figure 1** Inhibition of Akt signaling results in $G_1$ arrest with p15$^{INK4b}$ and p19$^{INK4d}$ expression. (**a**) 293T cells were treated with medium alone (Cont.), 100 nM Wortmannin (Wort.) or 50 μM Celecoxib (Celeco.). After a 24-h treatment, nuclear lysates were isolated and subjected to western blot analysis with the indicated antibodies. (**b**) 293T, HepG2 and Raji cells were treated with (+) or without (−) 50 μM LY294002 for 24 h and then analysed by western blot as described in (**a**). The asterisk indicates background band. (**c**) 293T, HepG2 and Raji cells were treated with (+) or without (−) 50 μM LY294002 for 6 h and then analysed by RT–PCR. (**d**) 293T cells were treated with (+) or without (−) 50 μM LY294002 for 24 h, and then CDK4 or CDK6 protein was immunoprecipitated from the nuclear lysates. CDK4 and CDK6 activities were analysed by *in vitro* kinase assay using recombinant C-terminal Rb as the substrate. (**e**) 293T, HepG2 and Raji cells were treated with (LY294002) or without (control) 50 μM LY294002 for 24 h. Cellular DNA contents were determined by flow cytometry. The percentage of the $G_1$ phase is the average of three independent experiments (inset). CDK, cyclin-dependent kinase; RT, reverse transcription.

*In vitro* kinase assay revealed that LY294002 downregulated the kinase activities of both CDK4 and CDK6 because CDK4/6-mediated phosphorylation of retinoblastoma (Rb) protein was downregulated by LY294002 treatment compared with non-treatment (Figure 1d). To examine the effects of LY294002 on cell-cycle progression, we performed flow cytometry. When 293T, HepG2 and Raji cells were treated with LY294002 for 24 h, increase in the $G_1$-arrested cell population was observed in each cell line (Figure 1e). These results suggest that suppressing the Akt signaling pathway by PI3K and PDK1 inhibitors may cause $G_1$ arrest by upregulating $p15^{INK4b}$ and $p19^{INK4d}$ expression.

### *FOXOs enhance* $p15^{INK4b}$ *and* $p19^{INK4d}$ *transcription*

We next demonstrated the upregulation of $p15^{INK4b}$ and $p19^{INK4d}$ by specifically inhibiting the Akt signaling pathway. After transfecting wild type (WT)- or dominant-negative (AAA)-*akt* cDNAs into 293T or HepG2 cells, we examined the expression levels of INK4 family mRNAs and proteins by means of RT–PCR and western blot analysis. The mRNA levels of the $p15^{INK4b}$ and $p19^{INK4d}$ genes were increased in the AAA-*akt* transfectants compared with that in empty vector transfectants (Mock) (Figure 2a). Conversely, these mRNA levels were downregulated in WT-*akt*-transfected cells. No change in $p16^{INK4a}$ and $p18^{INK4c}$ mRNA levels was observed in either transfectant (Figure 2a). In parallel with these results, we found an increase in $p15^{INK4b}$ and $p19^{INK4d}$ protein expression in AAA-*akt* transfectants and a decrease in these protein expression in WT-*akt* transfectants (Figure 2b).

FOXOs are downstream transcription factors of the Akt signaling pathway and are inactivated by it in a phosphorylation-dependent cytoplasmic translocation (Brunet *et al*., 1999; Woods and Rena, 2002). To confirm this phenomenon, we performed western blot analysis using the cytoplasmic and nuclear lysates from empty vector (Mock) or WT- or AAA-*akt* transfectants. The nuclear expression of both FOXO1a and FOXO3a decreased in WT-*akt* transfectants compared with that in mock transfectants, whereas the nuclear expression of both proteins increased in AAA-*akt* transfectants (Supplementary Figure S1). Next, to evaluate the association between FOXOs and $p15^{INK4b}$ or $p19^{INK4d}$ gene expression, we monitored $p15^{INK4b}$ and $p19^{INK4d}$ mRNA and protein expressions in WT or mutated FOXO1a- or FOXO3a-expressing cells. In the experiments, we used the active form (AAA, the mutant lacks the three Akt phosphorylation sites for nuclear export) and the inactive form (HR, the mutant lacks the

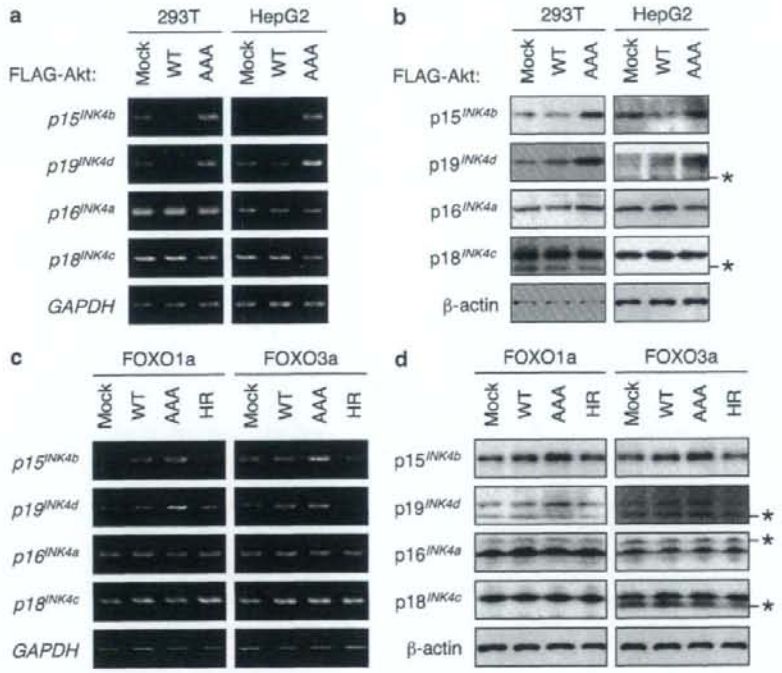


**Figure 2** Involvement of Akt and FOXOs in $p15^{INK4b}$ and $p19^{INK4d}$ expression. (**a** and **b**) 293T and HepG2 cells were transfected with a pFLAG-CMV-2 vector encoding none (Mock) or WT- or AAA-Akt. After transfection for 24 h, RT–PCR (**a**) or western blot (**b**) analyses were performed as described in Figure 1. The asterisks indicate background bands. (**c** and **d**) 293T cells were transfected with a pcDNA3 vector encoding none (Mock) or WT-, AAA- or HR-FOXO1a/3a. After transfection for 24 h, RT–PCR (**c**) or western blot (**d**) analyses were performed as described above. The asterisks indicate background bands. CMV, cytomegalovirus; FOXO, Forkhead box O; RT, reverse transcription; WT, wild type.

transcriptional ability because of its inability to bind to DNA) of FOXOs. Overexpression of WT- or AAA-FOXOs in 293T cells induced p15$^{INK4b}$ and p19$^{INK4d}$ mRNA and protein expressions (Figures 2c and d). Because neither HR-FOXO1a nor HR-FOXO3a had any effect on p15$^{INK4b}$ and p19$^{INK4d}$ mRNA and protein expressions (Figures 2c and d), transcriptional activities of FOXO1a and FOXO3a appeared to be essential for the expressions. The expression levels of p16$^{INK4a}$ and p18$^{INK4c}$ were unaffected by FOXO expression.

*FOXOs bind to* p15$^{INK4b}$ *and* p19$^{INK4d}$ *promoter regions and upregulate their transcription*

FOXOs are known to regulate transcription of *FasL* and *insulin-like growth factor-binding protein 1* (*IGF-BP1*) (Cichy *et al*., 1998; Brunet *et al*., 1999; Suhara *et al*., 2002). From these findings, FOXO consensus binding sites are reported as shown in Figure 3a (Brunet *et al*., 1999; Rokudai *et al*., 2002). We searched the Forkhead-responsive elements (FHREs) in the promoter regions of *p15$^{INK4b}$* and *p19$^{INK4d}$* genes. In the *p15$^{INK4b}$* promoter region, we found three overlapping domains highly homologous to FOXO consensus-binding sites (Figures 3a and b). We also found a domain that possessed high homology to a FOXO consensus-binding site in the *p19$^{INK4d}$* promoter region (Figures 3a and b).

To prove that FOXOs bound to the predicted sites, we performed electronic mobility shift assay (EMSA) with double-stranded oligonucleotides containing the FHREs in the *p15$^{INK4b}$* (WT-*p15*) or *p19$^{INK4d}$* gene (WT-*p19*). As expected, we could detect the mobility-shifted bands by incubating each oligonucleotide with nuclear extracts from WT-FOXO1a- or WT-FOXO3a-overexpressing 293T cells (Figures 3c and d). The FOXO1a binding to the WT-*p15* or WT-*p19* oligonucleotide was specific because the mobility-shifted bands were not detected in the presence of 100-fold excess of each competitor (unlabeled DNA), in incubation with nuclear extracts from HR-*FOXO1a* transfectants, or in incubation with the mutated *p15* or *p19* oligonucleotide (Mut-*p15* or Mut-*p19*, in which three nucleotides in the predicted FHREs were mutated; Figure 3c). Similar results suggested that FOXO3a binding to WT-*p15* or WT-*p19* oligonucleotide was specific (Figure 3d). To examine further the FOXO1a binding to conserved FHREs in *p15$^{INK4b}$* and *p19$^{INK4d}$* promoter regions in 293T cells, we performed chromatin immunoprecipitation assay in FLAG-tagged WT-, AAA- or HR-*FOXO1a* transfectants. WT- and AAA-FOXO1a bound

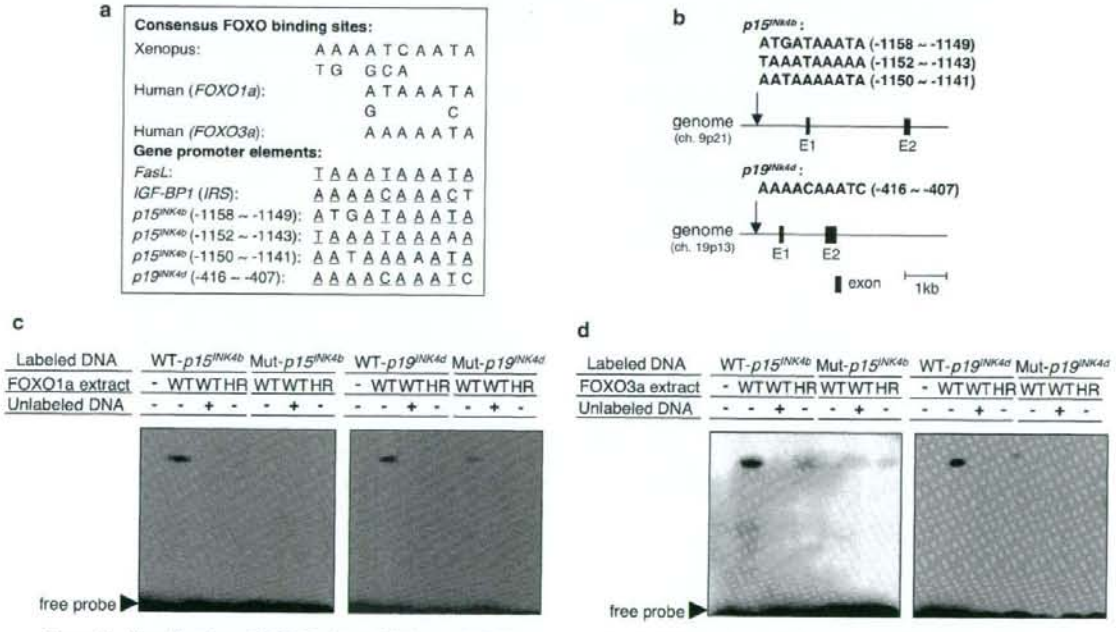


**Figure 3** Identification of FHREs in *p15$^{INK4b}$* or *p19$^{INK4d}$* gene promoter. (**a**) Comparison of the reported Xenopus and human consensus FHREs and the FHREs found in *FasL*, *IGF-BP1* (*IRS*), *p15$^{INK4b}$* or *p19$^{INK4d}$* promoter. The underlined nucleotides matched the predicted FOXO consensus sequence. (**b**) Genomic structure of the *p15$^{INK4b}$* or *p19$^{INK4d}$* gene. Black boxes indicate the locations and relative sizes of the exons. The locations of the potential FOXO-binding sequences are indicated on the upstream portion of exon 1 (E1). (**c** and **d**) Nuclear extracts from 293T cells that had been transfected with a pcDNA3 vector encoding none (−) or WT- or HR-FOXO1a/3a were incubated with biotin-labeled double-stranded WT- or Mut-*p15$^{INK4b}$* oligonucleotides (left panels) or WT- or Mut-*p19$^{INK4d}$* oligonucleotides (right panels). In some experiments, reactions were performed in the presence (+) or absence (−) of a 100-fold excess of unlabeled WT-*p15$^{INK4b}$* (left panels) or WT-*p19$^{INK4d}$* (right panels) oligonucleotides. DNA-protein complexes were separated by polyacrylamide gel electrophoresis and visualized by horseradish peroxidase-conjugated streptavidin. FHRE, forkhead-responsive element; FOXO, Forkhead box O; IGF-BP1, insulin-like growth factor-binding protein 1; WT, wild type.

to FHREs of *p15*$^{INK4b}$ and *p19*$^{INK4d}$ promoter regions, whereas HR-FOXO1a could not bind to the elements (Supplementary Figure S2). These results indicate that nuclear FOXOs exhibiting DNA-binding ability can specifically bind to the FHREs of *p15*$^{INK4b}$ and *p19*$^{INK4d}$ promoters *in vitro* and *in vivo*.

To confirm the involvement of FOXOs in *p15*$^{INK4b}$ and *p19*$^{INK4d}$ transcription, we constructed pGL3 promoter vectors containing a 1560-bp DNA fragment from the upstream portion of exon 1 of the *p15*$^{INK4b}$ gene (*p15*) and a 975-bp DNA fragment from the upstream portion of exon 1 of *p19*$^{INK4d}$ genes (*p19*), both of which contained the putative FHREs. The pGL3 reporter plasmids were transfected into 293T cells together with a pcDNA3 vector encoding nothing (Mock) or WT-, AAA- or HR-FOXO1a. As shown in Figure 4a, WT- and AAA-FOXO1a expression significantly increased luciferase activities of *p15* and *p19*. However, HR-FOXO1a expression did not affect reporter activities. To confirm further the role of putative FHREs in *p15*$^{INK4b}$ and *p19*$^{INK4d}$ gene expressions, we generated pGL3 reporter vectors containing four-tandem copies of the putative FOXO-responsive element of *p15*$^{INK4b}$ gene (WT-*p15*) or five-tandem copies of the element of *p19*$^{INK4d}$ gene (WT-*p19*). We also generated pGL3 reporter vectors containing mutated FHREs (Mut-*p15* and Mut-*p19*). Expression of WT- or AAA-FOXO1a, but not HR-FOXO1a, significantly enhanced the reporter activities of WT-*p15* and WT-*p19* (Figure 4b). We obtained similar results in the previously reported FHREs of *IGF-BP1* gene (*IRS-1*) (Figure 4b). The reporter activities, however, were not observed in the cells transfected with Mut-*p15* and Mut-*p19* (Figure 4b). By transfecting *FOXO3a*, we obtained similar results (Figure 4c). From these results, we conclude that FOXOs are involved in *p15*$^{INK4b}$ and *p19*$^{INK4d}$ gene transcription via binding to the identified FHREs.

We next examined the role of Akt in *p15*$^{INK4b}$ and *p19*$^{INK4d}$ gene expression. 293T cells were transfected with *FOXOs* together with a pFLAG-CMV-2 vector containing nothing (Mock) or WT- or AAA-Akt. Overexpression of WT-Akt slightly suppressed the WT-FOXO1a- or WT-FOXO3a-induced reporter activities of WT-*p15* and WT-*p19* (Figures 5a and b). Neither WT- nor AAA-Akt affected the AAA-FOXO-induced activation of luciferase (Figures 5a and d). Specific inhibition of the Akt signaling pathway by AAA-Akt expression significantly enhanced luciferase activity of WT-*p15* and WT-*p19* in both WT-FOXO1a and WT-FOXO3a transfectants (Figures 5a and b). These results suggest that Akt constitutively suppresses FOXO-induced *p15*$^{INK4b}$ and *p19*$^{INK4d}$ transcription in 293T cells.

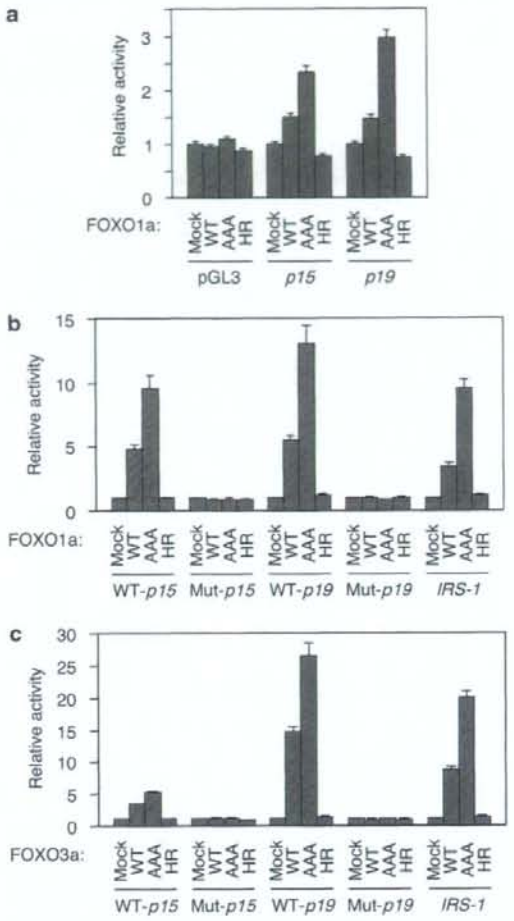


**Figure 4** Regulation of *p15*$^{INK4b}$ and *p19*$^{INK4d}$ gene transcription by FOXOs. (**a**) 293T cells were transfected with a pGL3 vector containing none (pGL3), a 1560-bp DNA fragment from the *p15*$^{INK4b}$ promoter region (*p15*), or a 975-bp DNA fragment from the *p19*$^{INK4d}$ promoter region (*p19*), together with a pcDNA3 vector containing none (Mock) or WT-, AAA- or HR-FOXO1a. A phRL-TK plasmid was also transfected as a transfection efficiency control. After 24 h of transfection, luciferase activities were measured with the dual-luciferase reporter assay system. (**b** and **c**) 293T cells were transfected with a pGL3 vector containing tandem copies of the oligonucleotide possessing the potential FOXO-binding sequence in the *p15*$^{INK4b}$ gene (WT-*p15*) or its mutant sequence (Mut-*p15*), the sequence in the *p19*$^{INK4d}$ gene (WT-*p19*) or its mutant sequence (Mut-*p19*), or the sequence in the *IGF-BP1* gene (*IRS-1*). 293T cells were also transfected with a pcDNA3 vector encoding none (Mock) or WT-, AAA- or HR-FOXO1a/3a. A phRL-TK plasmid was also co-transfected as a transfection efficiency control. After transfection for 24 h, luciferase activities were measured with the dual-luciferase reporter assay system. FOXO, Forkhead box O; WT, wild type.

### p15$^{INK4b}$ *or* p19$^{INK4d}$ *null MEFs show reduced responsiveness to LY294002-mediated* $G_1$ *arrest*

We first examined p15$^{INK4b}$ and p19$^{INK4d}$ expression levels in immortalized WT MEFs, *p15*$^{INK4b}$ knockout MEFs (*INK4b*$^{-/-}$ MEFs) or *p19*$^{INK4d}$ knockout MEFs (*INK4d*$^{-/-}$ MEFs) treated with or without LY294002 for 24 h. As expected, *INK4b*$^{-/-}$ MEFs did not express p15$^{INK4b}$, whereas *INK4d*$^{-/-}$ MEFs lacked p19$^{INK4d}$ expression (Figure 6a). LY294002 treatment suppressed PI3K activity (Supplementary Figure S3) and induced p27$^{KIP1}$ expression (Figure 6a) in each cell line. Suppression of Akt signaling pathway by LY294002 upregulated

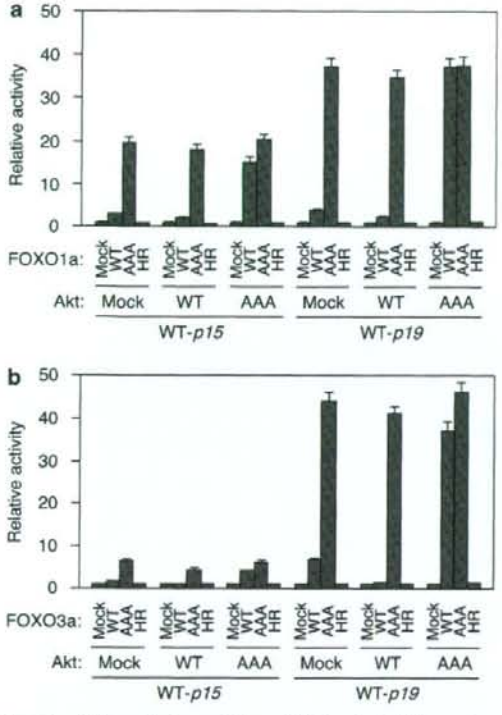


**Figure 5** Akt negatively regulates $p15^{INK4b}$ and $p19^{INK4d}$ gene transcription by phosphorylating and inactivating FOXOs. (**a** and **b**) 293T cells were co-transfected with a pGL3 vector containing tandem copies of the oligonucleotide that contained the potential FOXO-binding sequence from the $p15^{INK4b}$ (WT-*p15*) or $p19^{INK4d}$ gene (WT-*p19*) together with a phRL-TK plasmid as a transfection efficiency control. 293T cells were also transfected with a pcDNA3 vector encoding none (Mock) or WT-, AAA- or HR-FOXO1a/3a together with a pFLAG-CMV-2 vector encoding none (Mock) or WT- or AAA-Akt. After a 24-h transfection, luciferase activities were measured with the dual-luciferase reporter assay system. CMV, cytomegalovirus; FOXO, Forkhead box O; WT, wild type.

$p15^{INK4b}$ expression in WT and *INK4d*$^{-/-}$ MEFs, whereas it upregulated $p19^{INK4d}$ expression in WT and *INK4b*$^{-/-}$ MEFs (Figure 6a). Under the condition, we estimated CDK4 and CDK6 kinase activities. In WT MEFs, LY294002 suppressed both CDK4 and CDK6 kinase activities (Figure 6b). In contrast, LY294002 slightly inhibited CDK4 activity but not CDK6 activity in *INK4b*$^{-/-}$ and *INK4d*$^{-/-}$ MEFs (Figure 6b). Next, to determine the role of $p15^{INK4b}$ and $p19^{INK4d}$ in $G_1$ arrest caused by Akt inactivation, we analysed the cell cycle using flow cytometry after treatment of the immortalized WT MEFs, *INK4b*$^{-/-}$ MEFs or *INK4d*$^{-/-}$ MEFs with LY294002 for 24 h. Treatment of WT MEFs with LY294002 greatly increased the cell number in the $G_1$-arrested cell population, compared with untreated cells (Figures 6c and d). By contrast, cell-cycle pattern was almost the same in *INK4b*$^{-/-}$ and *INK4d*$^{-/-}$ MEFs before and after treatment with LY294002 (Figure 6c). LY294002-mediated accumulation of $G_1$-arrested cells could hardly be observed in *INK4b*$^{-/-}$ and *INK4d*$^{-/-}$ MEFs (Figure 6d). These results indicate that LY294002 induces $G_1$ arrest by enhancing $p15^{INK4b}$ and/or $p19^{INK4d}$ gene expressions and that FOXO activation by Akt inactivation is associated with those gene expressions.

## Discussion

The mutation of *PTEN* gene is observed with high frequency, to almost the same degree as tumor suppressor *p53* gene mutation in cancer cells (Bonneau and Longy, 2000), leads to aberrant activation of the Akt signaling pathway, and provides high cell survival and proliferating activities. FOXOs are direct targets of Akt and are negatively regulated by it in a phosphorylation-dependent manner (Brunet *et al*., 1999; Woods and Rena, 2002). FOXOs suppress cell proliferation with transcription of the apoptosis-related and/or cell-cycle inhibitor genes. $p27^{KIP1}$ is a target of transcription by FOXOs (Medema *et al*., 2000; Stahl *et al*., 2002), and it induces cell-cycle arrest in any phase. In addition, the functions of $p21^{CIP1}$ and $p27^{KIP1}$ are inhibited by Akt-dependent phosphorylation and translocation from nuclei to cytoplasm (Collado *et al*., 2000; Rodier *et al*., 2001; Zhou *et al*., 2001; Fujita *et al*., 2002). Thus, activation of the Akt signaling pathway can avoid cell-cycle arrest of cancer cells. Conversely, inhibitors of the pathway can induce the activation of these gene products and eliminate cell-cycle progression. In fact, the PI3K inhibitor LY294002 has been observed to induce both $G_1$ and $G_2$/M arrests (Figure 1e; Collado *et al*., 2000). According to previous studies, LY294002-induced $G_1$ arrest is considered to be due to activation of $p21^{CIP1}$ and $p27^{KIP1}$, whereas $G_2$/M arrest by the inhibitor may occur as a result of WEE1Hu activation in addition to $p21^{CIP1}$ and $p27^{KIP1}$ (Collado *et al*., 2000; Rodier *et al*., 2001; Zhou *et al*., 2001; Fujita *et al*., 2002; Katayama *et al*., 2005).

Matsushima-Nishiu *et al*. (2001) have shown that adenoviral transduction of the *PTEN* gene product induces $p15^{INK4b}$ mRNA expression as same as $p27^{KIP1}$ mRNA expression, as seen on DNA microarray and RT–PCR analyses. However, the molecular mechanisms of PTEN-induced $p15^{INK4b}$ have not been clarified. In this study, we then tried to examine the regulatory mechanisms of $p15^{INK4b}$ expression by the Akt signaling pathway. Treatment with inhibitors against Akt signaling pathway induced the $p15^{INK4b}$ gene product and simultaneously upregulated $p19^{INK4d}$ gene product (Figure 1). The dominant-negative form of Akt or WT- and active-FOXOs also induced $p15^{INK4b}$ and $p19^{INK4d}$ expression (Figure 2). These data indicate that $G_1$ arrest induced by inhibiting the Akt signaling pathway is caused by $p15^{INK4b}$ and $p19^{INK4d}$ expression in cooperation with $p21^{CIP1}$ and $p27^{KIP1}$ expression.

Further examination revealed that FOXOs bound to the promoter regions of the $p15^{INK4b}$ and $p19^{INK4d}$ genes and significantly upregulated their transcription (Figures 3–5). FOXO1a strongly activated $p15^{INK4b}$ transcription and $p19^{INK4d}$ transcription, while FOXO3a

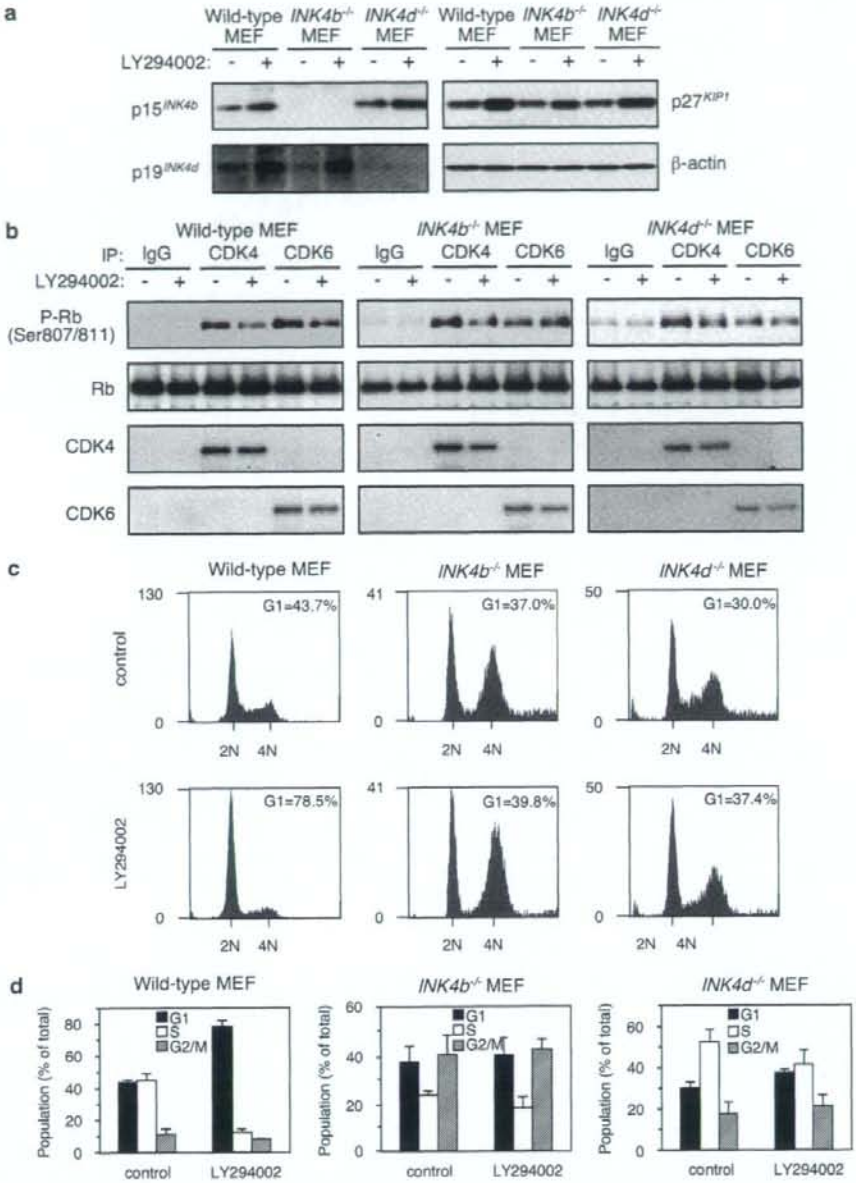


**Figure 6** Resistance to LY294002-induced $G_1$ arrest in *INK4b*$^{-/-}$ and *INK4d*$^{-/-}$ MEFs. (**a**) Immortalized wild-type, *INK4b*$^{-/-}$ or *INK4d*$^{-/-}$ MEFs were treated with (+) or without (−) 50 μM LY294002 for 24 h. Nuclear lysates from the cells were isolated and subjected to western blot analysis with the indicated antibodies. (**b**) Wild-type, *INK4b*$^{-/-}$ or *INK4d*$^{-/-}$ MEFs were treated with (+) or without (−) 50 μM LY294002 for 24 h, and then CDK4 or CDK6 protein was immunoprecipitated from the nuclear lysates. CDK4 and CDK6 activities were analysed by *in vitro* kinase assay using recombinant C-terminal Rb as the substrate. (**c**) Wild-type, *INK4b*$^{-/-}$ or *INK4d*$^{-/-}$ MEFs were treated with (lower panels) or without (upper panels) 50 μM LY294002. After treatment for 24 h, cellular DNA contents were determined by flow cytometry. The percentage of $G_1$ phase cells described in each panel is the average of three independent experiments (inset). (**d**) The percentage of $G_1$, S and $G_2$/M cell-cycle population was calculated from three independent experiments shown in (**c**). Each vertical bar represents the s.d. of the experiments. MEFs, mouse embryonic fibroblasts.

showed higher *p19*$^{INK4d}$ transcription activity than *p15*$^{INK4b}$ transcription activity (Figure 4). These results indicate that *p19*$^{INK4d}$ transcription is mediated by both FOXO1a and FOXO3a, but *p15*$^{INK4b}$ transcription may be regulated primarily by FOXO1a. Furthermore, WT-Akt slightly decreased WT-FOXO-induced activation of

luciferase, whereas dominant-negative Akt clearly enhanced luciferase activity in WT-FOXO-transfected 293T cells. Overexpression of WT- or AAA-Akt did not affect AAA-FOXO-induced activation of luciferase. Therefore, Akt suppressed the FOXO-mediated *p15$^{INK4b}$* and *p19$^{INK4d}$* gene transcription by phosphorylation. Although LY294002 arrested the cell cycle at the $G_1$ phase in 293T, HepG2, Raji and WT MEF cells (Figures 1 and 6), $G_1$ arrest could not be observed in *INK4b$^{-/-}$* or *INK4d$^{-/-}$* MEFs (Figure 6). Hence, induction of p15$^{INK4b}$ and p19$^{INK4d}$ expression by FOXOs is a critical event in LY294002-induced $G_1$ cell-cycle arrest.

In the present study, we used four different cell lines, 293T, HepG2, Raji and MEF. Rb is a substrate of CDK4/6/2 and a negative regulator of cell cycle. At $G_1$/S transition, CDK4/6/2-mediated phosphorylation and inactivation of Rb is necessary for cell-cycle progression. In 293T cells, Rb dysfunctions by adenoviral protein and SV40T antigen, and 293T cells exhibit resistance to Rb-mediated $G_1$ arrest. Actually, LY294002 slightly arrested cell cycle at $G_1$ phase in 293T cells (Figure 1e). In contrast, LY294002 drastically induced $G_1$ arrest in HepG2, Raji and WT MEF cells (Figures 1e and 6), which contain normal Rb as a tumor suppressor gene product (Puisieux *et al*., 1993; Wells *et al*., 2003). These findings suggest that LY294002-mediated $G_1$ arrest is induced by Rb-dependent and -independent pathways. In Rb-independent $G_1$ arrest, a key molecule may be Smad3. Smad3 has a key function in mediating transforming growth factor-β signaling pathway that inhibits cell-cycle progression at $G_1$ phase. Smad3 upregulates p15$^{INK4b}$ expression and downregulates c-Myc expression, resulting in cell-cycle arrest at $G_1$ phase (Matsuura *et al*., 2004). CDK4/2 phosphorylates and inactivates Smad3 and prevents $G_1$ cell-cycle arrest (Matsuura *et al*., 2004). LY294002 may also activate Smad3 and inhibit cell-cycle progression at $G_1$ phase in cooperation with FOXO-p15$^{INK4b}$/p19$^{INK4d}$-CDK pathway, especially in 293T cells.

Methylation of the CpG island, deletion and mutation in chromosome (Ch.) 9p21, which codes p15$^{INK4b}$, p16$^{INK4a}$ and p14$^{ARF}$ genes, are often observed in many cancers (Ruas and Peters, 1998). p14$^{ARF}$ is an activator of p53 and indirectly induces p21$^{CIP1}$ expression (Stott *et al*., 1998). Defect of Ch. 9p21 therefore causes aberrant cell-cycle progression in cancer cells. In contrast, deletions or rearrangement of *p18$^{INK4c}$* (Ch. 1p32) and *p19$^{INK4d}$* (Ch. 19p13) are hardly observed (Zariwala *et al*., 1996). Especially, mutation of *p19$^{INK4d}$* is extremely rare. Hence, it is useful for cancer chemotherapy to induce p18$^{INK4c}$- and/or p19$^{INK4d}$-dependent $G_1$ arrest in both *p15$^{INK4b}$*- and *p16$^{INK4a}$*-defective cancer cells.

Mdm2 is a ubiquitin E3 ligase for p53. Akt also phosphorylates and translocates Mdm2 from the cytoplasm into the nucleus, resulting in promoting p53 degradation and cell-cycle arrest (Mayo and Donner, 2001). In the cells containing normal p53, suppression of Akt signaling pathway upregulates p53 expression and abrogates cell-cycle progression in this mechanism. In contrast, it is difficult to induce cell-cycle arrest via p53-p21$^{CIP1}$ pathway in p53-defective cancer cells. p53 of 293T cells also dysfunctions by SV40T antigen, but LY294002 can abolish cell-cycle progression with upregulating p15$^{INK4b}$, p19$^{INK4d}$ and p27$^{KIP1}$ and with inhibiting CDK4/6 kinase activities. Therefore, the inhibitors against Akt signaling pathway may be useful for many cancer cells regardless of *p53* mutation.

In summary, we demonstrate that FOXOs arrest the cell cycle at the $G_1$ phase by direct induction of p15$^{INK4b}$ and p19$^{INK4d}$ expression through transcriptional mechanisms. Conversely, Akt suppresses p15$^{INK4b}$ and p19$^{INK4d}$ expression by Akt-dependent phosphorylation and inactivation of FOXOs.

## Materials and methods

*Reagents and cell-culture conditions*

Wortmannin, LY294002 and Celecoxib were purchased from Merck Calbiochem (San Diego, CA, USA), Sigma (St Louis, MO, USA) and LKT Laboratories (St Paul, MN, USA), respectively. Human embryonic kidney 293T cells and human hepatoblastoma HepG2 cells were cultured in Dulbecco's modified Eagle's medium supplemented with 10% fetal bovine serum. Human Burkitt lymphoma Raji cells were cultured in RPMI-1640 supplemented with 10% fetal bovine serum. *INK4b$^{-/-}$* and *INK4d$^{-/-}$* MEFs were kindly provided by Dr Mariano Barbacid (Centro Nacional de Investigaciones Oncológicas, Madrid, Spain) and Drs Martine F Roussel and Charles J Sherr (St Jude Children's Research Hospital, Memphis, TN, USA), respectively, and were cultured as described previously (Latres *et al*., 2000; Zindy *et al*., 2000). These MEFs were immortalized by cultivating them for 2–3 months in our laboratory and then were used for some analyses.

*Plasmids*

Human WT and dominant-negative (AAA, K179A/T308A/S473A) *akt1* cDNAs in a pFLAG-CMV-2 vector (Sigma) were established in our laboratory (Fujita *et al*., 2002). Human FLAG-tagged WT-*FOXO1a*, AAA (T24A/S256A/S319A)-*FOXO1a* and HR (H215R)-*FOXO1a* in a pcDNA3 vector (Invitrogen, San Diego, CA, USA) were kindly provided by Drs Eric D Tang (University of Michigan Medical School, Ann Arbor, MI, USA) and Frederic G Barr (University of Pennsylvania, School of Medicine, Philadelphia, PA, USA) (Tang *et al*., 1999). Human WT-*FOXO3a* cDNA in a pcDNA3 vector was generated by PCR with an IMAGE clone (ID: 4137370, Invitrogen) as a template. The AAA (T32A/S253A/S315A)-*FOXO3a* and HR (H212R)-*FOXO3a* cDNAs were accomplished using a QuickChange Site-Directed Mutagenesis Kit (Stratagene, La Jolla, CA, USA).

*Flow-cytometric analysis*

Cells were treated with 50 μM LY294002 for 24 h. Flow-cytometric analyses were performed as described previously (Katayama *et al*., 2005).

*Transient transfection and western blot analysis*

Cells were transfected with the appropriate plasmids using Superfect transfection reagent (Qiagen, Valencia, CA, USA). Western blot analysis was performed as described previously (Katayama *et al*., 2005). Nuclear fraction was extracted using an NE-PER extraction kit (Pierce, Rockford, IL, USA). We

used antibodies to p16$^{INK4a}$ (F-12), p15$^{INK4b}$ (K-18) or p18$^{INK4c}$ (M-20) (Santa Cruz Biotechnology, Santa Cruz, CA, USA); an antibody to human p19$^{INK4d}$ (DCS-100) (Lab Vision, Fremont, CA, USA); an antibody to mouse p19$^{INK4d}$ (ZP002) (Invitrogen); an antibody to β-actin (AC-15) (Sigma); and antibodies to p21$^{CIP1}$ or p27$^{KIP1}$ (BD Biosciences, San Jose, CA, USA).

*Semiquantitative RT–PCR analysis*
We extracted total RNA from cells with Trizol reagent (Invitrogen). RT–PCR experiments were performed as described in Supplementary Materials and methods.

In vitro *CDK assay*
Cells were treated with or without 50 μM LY294002 for 24 h, and then endogenous CDK4 and CDK6 were immunoprecipitated from the cell lysates using antibodies to CDK4 (C-22) and CDK6 (C-21) (Santa Cruz Biotechnology), respectively. *In vitro* CDK assay was performed as described previously (Ogasawara *et al*., 2004). Recombinant C-terminal Rb (Cell Signaling Technology, Beverly, MA, USA) and immunoprecipitated CDK4 and CDK6 were detected by western blot analysis. We used antibodies to Rb and phospho-Rb (Ser807/811; Cell Signaling Technology); and antibodies to CDK4 (DCS-35) and CDK6 (B-10; Santa Cruz Biotechnology).

*Cloning of pGL3 promoter vectors*
The 1560-bp DNA fragment of the p15$^{INK4b}$ promoter region, −1557 to +3 and 975-bp DNA fragment of p19$^{INK4d}$ promoter region, −975 to −1, containing a potential FOXO-binding sequence were amplified by PCR and were cloned into the pGL3 promoter vector (Promega, Madison, WI, USA) as described in Supplementary Materials and methods.

*Cloning of pGL3 reporter vectors containing tandem copies of the putative FOXO-responsive element*
Double-stranded oligonucleotides containing a potential FOXO-binding sequence were generated by PCR and were ligated into the pGL3 promoter vector as described in Supplementary Materials and methods. The pGL3-3xIRS vector (IRS-1) was reported previously (Rokudai *et al*., 2002).

*Electronic mobility shift assay*
293T cells were transfected with WT- or HR-*FOXO* cDNA, and the nuclear extractions of the cells were used in EMSA. The detailed experimental procedures were described in Supplementary Materials and methods.

*Chromatin immunoprecipitation assay*
293T cells were transfected with a pcDNA3 vector encoding none or FLAG-tagged WT-, AAA- or HR-FOXO1a. The detailed experimental procedures were described in Supplementary Materials and methods.

*Luciferase assay*
293T cells were co-transfected with a pGL3-promoter vector encoding none or FOXO consensus p15$^{INK4b}$, p19$^{INK4d}$ or IRS-1 sequence and a pcDNA3 vector encoding none or FOXO together with or without *akt1* cDNAs. Quantification of all luciferase activities was performed with a dual-luciferase reporter assay system (Promega). Activities were normalized by co-transfection of control thymidine kinase-driven *Renilla* luciferase plasmid phRL-TK (Promega).

*PI3K assay*
Cells were treated with 50 μM LY294002 for 24 h, and then PI3K activity was measured using the QTL lightspeed class I phosphoinositide 3-kinase (PI3K-α, PI3K-β, PI3K-δ and PI3K-γ) end point assay kit (QTL Biosystems, Santa Fe, NM, USA). The detailed experimental procedures were described in Supplementary Materials and methods.

**Acknowledgements**

This study was supported in part by special grants from the Ministry of Education, Culture, Sports, Science and Technology, Japan 17016012 and 18015008 (to TT and NF). NF is also supported by the Araki Memorial Foundation for Medical and Biochemical Researches, by the Vehicle Racing Commemorative Foundation and by the Uehara Memorial Foundation.

**References**

Bonneau D, Longy M. (2000). Mutation of the PTEN gene. *Hum Mutat* **16**: 109–122.

Brunet A, Bonni A, Zigmond MJ, Lin MZ, Juo P, Hu LS *et al*. (1999). Akt promotes cell survival by phosphorylating and inhibiting a forkhead transcription factor. *Cell* **96**: 857–868.

Cichy SB, Uddin S, Danilkovich A, Guo S, Klippel A, Unterman TG. (1998). Protein kinase B/Akt mediates effects of insulin on hepatic insulin-like growth factor-binding protein-1 gene expression through a conserved insulin response sequence. *J Biol Chem* **273**: 6482–6487.

Collado M, Medema RH, Garcia-Cao I, Dubuisson ML, Barradas M, Glassford J *et al*. (2000). Inhibition of the phosphoinositide 3-kinase pathway induces a senescence-like arrest mediated by p27$^{Kip1}$. *J Biol Chem* **276**: 21960–21968.

Fujita N, Sato S, Katayama K, Tsuruo T. (2002). Akt-dependent phosphorylation of p27$^{Kip1}$ promotes binding to 14-3-3 and cytoplasmic localization. *J Biol Chem* **277**: 28706–28713.

Katayama K, Fujita N, Tsuruo T. (2005). Akt/protein kinase B-dependent phosphorylation and inactivation of WEE1Hu promote cell cycle progression at $G_2$/M transition. *Mol Cell Biol* **25**: 5725–5737.

LaBaer J, Garrett MD, Stevenson LF, Slingerland JM, Sandhu C, Chou HS *et al*. (1997). New functional activities for the p21 family of CDK inhibitors. *Genes Dev* **11**: 847–862.

Latres E, Malumbres M, Sotillo R, Martin J, Ortega S, Martin-Caballero J *et al*. (2000). Limited overlapping roles of P15$^{INK4b}$ and P18$^{INK4c}$ cell cycle inhibitors in proliferation and tumorigenesis. *EMBO J* **19**: 3496–3506.

Matsushima-Nishiu M, Unoki M, Ono K, Tsunoda T, Minaguchi T, Kuramoto H *et al*. (2001). Growth and gene expression profile analyses of endometrial cancer cells expressing exogenous PTEN. *Cancer Res* **61**: 3741–3749.

Matsuura I, Denissova NG, Wang G, He D, Long J, Liu F. (2004). Cyclin-dependent kinases regulate the antiproliferative function of Smads. *Nature* **430**: 226–231.

Mayo LD, Donner DB. (2001). A phosphatidylinositol 3-kinase/Akt pathway promotes translocation of Mdm2 from the cytoplasm to the nucleus. *Proc Natl Acad Sci USA* **98**: 11598–11603.

Medema RH, Kops GJ, Bos JL, Burgering BM. (2000). AFX-like forkhead transcription factors mediate cell-cycle regulation by Ras and PKB thorough p27$^{Kip1}$. *Nature* **404**: 782–787.

Ogasawara T, Kawaguchi H, Jinno S, Hoshi K, Itaka K, Takato T *et al*. (2004). Bone morphogenetic protein 2-induced osteoblast differentiation requires Smad-mediated down-regulation of Cdk6. *Mol Cell Biol* **24**: 6560–6568.

Puisieux A, Galvin K, Troalen F, Bressac B, Marcais C, Galun E *et al*. (1993). Retinoblastoma and p53 tumor suppressor genes in human hepatoma cell lines. *FASEB J* **7**: 1407–1413.

Rodier G, Montagnoli A, Di Marcotullio L, Coulombe P, Draetta GF, Pagano M *et al.* (2001). p27 cytoplasmic localization is regulated by phosphorylation on Ser10 and is not a prerequisite for its proteolysis. *EMBO J* **20**: 6672–6682.

Rokudai S, Fujita N, Kitahara O, Nakamura Y, Tsuruo T. (2002). Involvement of FKHR-dependent TRADD expression in chemotherapeutic drug-induced apoptosis. *Mol Cell Biol* **22**: 8695–8708.

Ruas M, Peters G. (1998). The p16$^{INK4a}$/CDKN2A tumor suppressor and its relatives. *Biochim Biophys Acta* **1378**: F115–F177.

Sherr CJ, Roberts JM. (1995). Inhibitors of mammalian G1 cyclin-dependent kinases. *Genes Dev* **9**: 1149–1163.

Stahl M, Dijkers PF, Kops GJ, Les SM, Coffer PJ, Burgering BM *et al.* (2002). The forkhead transcription factor FoxO regulates transcription of p27$^{Kip1}$ and Bim in response to IL-2. *J Immunol* **168**: 5024–5031.

Stott FJ, Bates S, James MC, McConnell BB, Starborg M, Brookes S *et al.* (1998). The alternative product from the human CDKN2A locus, p14$^{ARF}$, participates in a regulatory feedback loop with p53 and MDM2. *EMBO J* **17**: 5001–5014.

Suhara T, Kim HS, Kirshenbaum LA, Walsh K. (2002). Suppression of Akt signaling induces Fas ligand expression: involvement of caspase and Jun kinase activation in Akt-mediated Fas ligand regulation. *Mol Cell Biol* **22**: 680–691.

Tang ED, Nunez G, Barr FG, Guan KL. (1999). Negative regulation of the forkhead transcription factor FKHR by Akt. *J Biol Chem* **274**: 16741–16746.

Tsuruo T, Naito M, Tomida A, Fujita N, Mashima T, Sakamoto H *et al.* (2003). Molecular targeting therapy of cancer: drug resistance, apoptosis and survival signal. *Cancer Sci* **94**: 15–21.

Vanhaesebroeck B, Alessi DR. (2000). The PI3K-PDK1 connection: more than just a road to PKB. *Biochem J* **346**: 561–576.

Wells J, Yan PS, Cechvala M, Huang T, Farnham PJ. (2003). Identification of novel pRb binding sites using CpG microarrays suggests that E2F recruits pRb to specific genomic sites during S phase. *Oncogene* **22**: 1445–1460.

Woods YL, Rena G. (2002). Effect of multiple phosphorylation events on the transcription factors FKHR, FKHRL1, and AFX. *Biochem Soc Trans* **30**: 391–397.

Zariwala M, Liu E, Xiong Y. (1996). Mutational analysis of the p16 family cyclin-dependent kinase inhibitors p15$^{INK4b}$ and p18$^{INK4c}$ in tumor-derived cell lines and primary tumors. *Oncogene* **12**: 451–455.

Zhou BP, Liao Y, Xia W, Spohn B, Lee MH, Hung MC. (2001). Cytoplasmic localization of p21Cip1/WAF1 by Akt-induced phosphorylation in HER-2/neu-overexpressing cells. *Nat Cell Biol* **3**: 245–252.

Zindy F, van Deursen J, Grosveld G, Sherr CJ, Roussel MF. (2000). *INK4d*-deficient mice are fertile despite testicular atrophy. *Mol Cell Biol* **20**: 372–378.

Supplementary Information accompanies the paper on the Oncogene website (http://www.nature.com/onc).

Annals of Oncology Advance Access published January 22, 2009

original article

Annals of Oncology
doi:10.1093/annonc/mdn705

# Phase III trial of docetaxel plus gemcitabine versus docetaxel in second-line treatment for non-small-cell lung cancer: results of a Japan Clinical Oncology Group trial (JCOG0104)

K. Takeda[1]*, S. Negoro[1,9], T. Tamura[2], Y. Nishiwaki[3], S. Kudoh[4], S. Yokota[5], K. Matsui[6], H. Semba[7], K. Nakagawa[8], Y. Takada[9], M. Ando[10], T. Shibata[11] & N. Saijo[3]

[1]Department of Clinical Oncology, Osaka City General Hospital, Osaka; [2]Department of Internal Medicine, National Cancer Center Hospital, Tokyo; [3]Division of Thoracic Oncology, National Cancer Center Hospital East, Kashiwa; [4]Department of Respiratory Medicine, Osaka City University Medical School, Osaka; [5]Division of Pulmonary Medicine, Tonoyama National Hospital, Toyonaka; [6]Department of Thoracic Malignancy, Osaka Prefectural Medical Center for Respiratory and Allergic diseases, Habikino; [7]Division of Respiratory Disease, Kumamoto Regional Medical Center, Kumamoto; [8]Department of Medical Oncology, Kinki University School of Medicine, Osaka-Sayama; [9]Department of Thoracic Oncology, Hyogo Cancer Center, Akashi; [10]Department of Preventive Services, Kyoto University School of Public Health, Kyoto; [11]JCOG Data Center, Clinical Trials and Practice Support Division, Center for Cancer Control and Information Services, National Cancer Center, Tokyo, Japan

Received 28 March 2008; revised 17 September 2008; accepted 8 October 2008

**Background:** This trial evaluated whether a combination of docetaxel and gemcitabine provides better survival than docetaxel alone in patients with previously treated non-small-cell lung cancer (NSCLC).

**Patients and methods:** Eligibility included pathologically or cytologically proven NSCLC, failure of one platinum-based regimen, performance status of zero or one, 20–75 years old, and adequate organ function. Patients received docetaxel 60 mg/m$^2$ (day 1) or docetaxel 60 mg/m$^2$ (day 8) and gemcitabine 800 mg/m$^2$ (days 1 and 8), both administered every 21 days until disease progression.

**Results:** Sixty-five patients participated in each arm. This trial was terminated early due to an unexpected high incidence of interstitial lung disease (ILD) and three treatment-related deaths due to ILD in the combination arm. Docetaxel plus gemcitabine compared with docetaxel-alone patients experienced similar grade and incidence of toxicity, except for ILD. No baseline factor was identified for predicting ILD. Median survival times were 10.3 and 10.1 months (one-sided $P = 0.36$) for docetaxel plus gemcitabine and docetaxel arms, respectively.

**Conclusion:** Docetaxel alone is still the standard second-line treatment for NSCLC. The incidence of ILD is higher for docetaxel combined with gemcitabine than for docetaxel alone in patients with previously treated NSCLC.

**Key words:** docetaxel, gemcitabine, non-small-cell lung cancer, platinum-refractory, second-line chemotherapy



## introduction

Lung cancer is the most common cancer worldwide, with an estimated 1.2 million new cases globally (12.3% of all cancers) and 1.1 million deaths (17.8% of all cancer deaths) in 2000 [1]. The estimated global incidence of non-small-cell lung cancer (NSCLC) in 2000 was ~1 million, which accounted for ~80% of all cases of lung cancer [1]. Treatment of advanced NSCLC is palliative; the aim is to prolong survival without leading to deterioration in quality of life [2]. The recommended first-line treatment of advanced NSCLC currently involves up to four cycles of platinum-based combination chemotherapy, with no single combination recommended over others [3]. Although this treatment improves survival rates, a substantial proportion of patients do progress and should be offered second-line treatment. With unsurpassed efficacy compared with other chemotherapeutic regimens or best supportive care [4, 5], docetaxel alone is the current standard as second-line chemotherapy for advanced NSCLC. The recommended regimen of docetaxel 75 mg/m$^2$ given i.v. every 3 weeks as second-line therapy has been associated with median survival times of 5.7–7.5 months [4, 5] and is also associated with better quality-of-life outcomes compared with best supportive care [2]. Docetaxel monotherapy for recurrent NSCLC after platinum-based chemotherapy has several limitations, however, including low response rates (7–11%), brief duration of disease control, and minimal survival advantage [4, 5].

Gemcitabine is also active against recurrent NSCLC after platinum-based chemotherapy [6]. Gemcitabine 1000 mg/m$^2$ once a week for 3 weeks every 28 days produced a 19% response rate in a phase II trial, and it shows significant activity mainly

*Correspondence to: Dr K. Takeda, 2-13-22 Miyakojimahondohri, Miyakojima-ku, Osaka 534-0021, Japan. Tel: +81-6-6929-1221; Fax: +81-6-6929-1090; E-mail: kkk-take@ga2.so-net.ne.jp

in patients previously responsive to chemotherapy [6]. Single-agent gemcitabine has a low toxicity profile and is well tolerated [6].

Docetaxel and gemcitabine have distinct mechanisms of action and nonoverlapping toxic effects except for neutropenia. Many studies of the combination of docetaxel and gemcitabine have been conducted in first- and second-line settings [7–16]. The following doses and schedule have been adopted in most studies: docetaxel 80–100 mg/m$^2$ on day 1 or 8 and gemcitabine 800–1000 mg/m$^2$ on days 1 and 8 or on days 1, 8, and 15. Furthermore, most studies required use of prophylactic granulocyte colony-stimulating factor (G-CSF) support.

In Japan, however, the recommended dose of docetaxel is 60 mg/m$^2$ every 3 weeks [17, 18]. Several studies to confirm the dose and schedule of this combination without prophylactic G-CSF support have been conducted in Japan [19–21]. Two studies recommended docetaxel 60 mg/m$^2$ on day 8 and gemcitabine 800 mg/m$^2$ on days 1 and 8, and another study recommended docetaxel 50 mg/m$^2$ on day 8 and gemcitabine 1000 mg/m$^2$ on days 1 and 8, without prophylactic G-CSF support, every 3 weeks. These studies demonstrated the consistent promising efficacy of this combination regimen. An objective response was observed in 28%–40% of patients, with a median survival time of 11.1–11.9 months and a 1-year survival rate of 41%–47%.

We conducted a multicenter, randomized, phase III trial to evaluate whether the combination regimen of docetaxel and gemcitabine provides better survival than docetaxel alone in patients with previously treated NSCLC.

## patients and methods

### patient selection

Eligible patients were 20–75 years of age, with histologically or cytologically confirmed stage IIIB (with malignant pleural effusion or contralateral hilar lymph node metastases) or stage IV NSCLC who had failed one platinum-based chemotherapy regimen previously. Patients who had received gemcitabine or docetaxel were excluded. Additional inclusion criteria included a Eastern Cooperative Oncology Group performance status of zero to one, and adequate organ function as indicated by white blood cell count ≥4000/μl, absolute neutrophil count ≥2000/μl, hemoglobin ≥9.5 g/dl, platelets ≥100 000/μl, aspartate aminotransferase (AST)/alanine amonotransferase (ALT) ≤2.5 times the upper limit of normal, total bilirubin ≤1.5 mg/dl, serum creatinine ≤1.2 mg/dl, and $PaO_2$ in arterial blood ≥70 torr. Asymptomatic brain metastases were allowed provided that they had been irradiated and were clinically and radiologically stable. Prior thoracic radiotherapy was allowed provided that treatment was completed at least 12 weeks before enrollment. Patients were excluded from the study if they had radiologically and clinically apparent interstitial pneumonitis or pulmonary fibrosis. All patients provided written informed consent, and the study protocol was approved by Japan Clinical Oncology Group (JCOG) Clinical Trial Review Committee and the institutional review board of each participating institution.

### treatment plan and dose modifications

Eligible patients were centrally registered at JCOG Data Center and were randomly assigned to either docetaxel 60 mg/m$^2$ as a 60-min i.v. infusion on day 1 or docetaxel 60 mg/m$^2$ as a 60-min i.v. infusion on day 8 plus gemcitabine 800 mg/m$^2$ as a 30-min i.v. infusion on days 1 and 8, using a minimization method with institutions and response to prior chemotherapy (progressive disease or not) as balancing factors. Patients receiving docetaxel were administered standard dexamethasone premedication (8 mg orally at the day before, on the day, and the day after docetaxel administration) as previously reported [7] and 50 mg of diphenhidramine 30 min before docetaxel administration. Recombinant human G-CSF was not given prophylactically. Chemotherapy cycles were repeated every 3 weeks until disease progression. Docetaxel was given before gemcitabine in the docetaxel plus gemcitabine regimen.

Dose adjustments were based mainly on hematologic parameters. The doses of docetaxel and gemcitabine were reduced by 10 and 200 mg/m$^2$, respectively, in subsequent cycles if chemotherapy-induced febrile neutropenia, grade 4 anemia, grade 4 thrombocytopenia, grade 4 leukopenia, or grade 4 neutropenia lasting for >3 days occurred in the absence of fever. Dose reductions were maintained for all subsequent cycles. Patients requiring more than one dose reduction were off-protocol treatment.

### baseline and follow-up assessments

Pretreatment evaluation included a complete medical history and physical examination, a complete blood count (CBC) test with differential and platelet count, standard biochemical profile, electrocardiogram, chest radiographs, computed tomographic scans of the chest, abdomen, and brain, magnetic resonance imaging, and a whole-body bone scan. During treatment, a CBC and biochemical tests were carried out weekly. A detailed medical history was taken and a complete physical examination with clinical assessment was carried out weekly to assess disease symptoms and treatment toxicity, and chest radiographs were done every treatment cycle. Toxicity was evaluated according to the National Cancer Institute Cancer—Common Toxicity Criteria Version 2 [22].

All patients were assessed for response by computed tomography scans after every two cycles of chemotherapy. Response Evaluation Criteria in Solid Tumors (RECIST) were used for the evaluation of response [23].

The progression-free survival (PFS) was calculated from the day of randomization until the day of the first evidence of disease progression or death. If the patient had no progression, PFS was censored at the day when no clinical progression was confirmed. Overall survival (OS) was measured from the day of randomization to death.

Disease-related symptoms were evaluated and scored at baseline and 6 weeks after the start of treatment with the seven-item Lung Cancer Subscale (LCS) of the Functional Assessment of Cancer Therapy-Lung version 4 [24], which were translated from English to Japanese. The questionnaire entries were listed as follows: 'I have been short of breath', 'I am losing weight', 'My thinking is clear', 'I have been coughing', 'I have a good appetite', 'I feel tightness in my chest', and 'Breathing is easy for me'. Patients scored using a five-point Likert scale (0–4) by themselves. The maximum attainable score of the LCS was 28, where the patient was considered to be asymptomatic.

### statistical analysis

The primary endpoint was OS; secondary endpoints were PFS, the overall response rate, disease-related symptoms, and toxicity profile. Based on previous trials evaluating the docetaxel [4, 5] and docetaxel plus gemcitabine [19–21] regimens, the present study was designed to detect a 12% difference of 1-year survival rate. To attain an 80% power at a one-sided significance level of 0.05, assuming 1-year survival of docetaxel arm as 35% with 1 year of follow-up after 2 years of accrual, 284 patients (142 per each arm) were required. Analyses were to be carried out with all randomized patients. Both the OS and PFS were estimated with the Kaplan–Meier method. The comparisons of OS and PFS between arms were assessed by the stratified log-rank test with a factor used at randomization, response to prior chemotherapy. Two interim analyses were planned after half of the patients were registered and the end of registration.

For the symptom analysis, changes of LCS from initial score were compared between arms using analysis of covariance with initial score as a covariate.

All analyses were carried out with SAS software release 8.2 (SAS Institute, Cary, NC).

## results

This trial was terminated early due to the unexpected high incidence of interstitial lung disease (ILD) and three treatment-related deaths due to ILD in the combination arm, which were identified by the Adverse Event Reporting system.

### patient characteristics

From January 2002 to September 2003, 130 patients with NSCLC who had failed prior platinum-based chemotherapy from 32 institutions were enrolled (Appendix). These patients were randomly assigned to docetaxel alone ($n = 65$) or docetaxel plus gemcitabine ($n = 65$). One patient died as a result of rapid progressive disease before chemotherapy administration, and one patient did not meet the entry criteria in the docetaxel arm. In addition, one patient did not meet the entry criteria in the docetaxel plus gemcitabine arm. All patients were included in the analysis of survival and PFS, and 64 docetaxel and 65 docetaxel plus gemcitabine patients were assessable for toxicity. Fifty-nine patients with measurable lesions by RECIST in the docetaxel arm and 57 eligible patients in docetaxel plus gemcitabine arm were assessable for response (Figure 1). Table 1 presents baseline patient characteristics.

The median number of cycles was 3 (range 0–6) and 2 (range 1–8) in the docetaxel and docetaxel plus gemcitabine arms, respectively. The median interval between cycles was 22 days for both arms.

### toxicity

This trial was terminated early due to the unexpected high incidence of ILD and three treatment-related deaths (4.6%) due to ILD in the docetaxel plus gemcitabine arm. These events were identified by the Adverse Event Reporting system. Thirteen (20.0%) patients receiving combination treatment suffered from all grades of ILD, whereas only two (3.1%) patients receiving docetaxel alone suffered from grades 1–2 ILD. Grades 2–4 ILD occurred in 16.9% of docetaxel plus gemcitabine patients, an unexpected high incidence rate. No risk factors were identified contributing to these pulmonary adverse events.

Toxicity was assessed in all patients who received at least one treatment cycle and in all cycles (Table 2). Overall, grades 3–4 neutropenia occurred in 55 docetaxel patients (85.9%) and 53 docetaxel plus gemcitabine patients (81.5%). Grades 3–4 anemia occurred in two patients (3.1%) and 12 patients (18.5%) treated with docetaxel alone and docetaxel plus

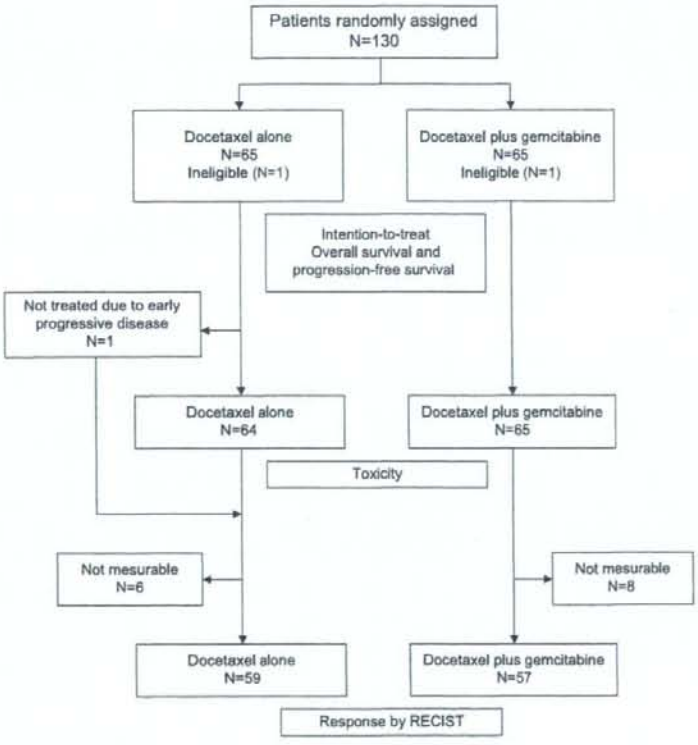


**Figure 1.** CONSORT diagram for the study.

**Table 1.** Patient characteristics

| | D arm | | DG arm | |
|---|---|---|---|---|
| | No. of patients | % | No. of patients | % |
| Patients enrolled | 65 | | 65 | |
| Age, years | | | | |
| Median | 62 | | 60 | |
| Range | 34–75 | | 34–74 | |
| Gender | | | | |
| Male | 48 | 73.8 | 51 | 78.5 |
| Female | 17 | 26.2 | 14 | 21.5 |
| ECOG PS | | | | |
| 0 | 20 | 30.8 | 21 | 32.3 |
| 1 | 45 | 69.2 | 44 | 67.7 |
| Histology | | | | |
| Squamous | 19 | 29.2 | 22 | 33.8 |
| Adenocarcinoma | 40 | 61.5 | 40 | 61.5 |
| Large cell | 4 | 6.2 | 3 | 4.6 |
| Others | 2 | 3.1 | 0 | 0 |
| Best response of prior chemotherapy | | | | |
| CR | 2 | 3.1 | 0 | 0 |
| PR | 38 | 58.5 | 40 | 61.5 |
| SD | 20 | 30.8 | 19 | 29.2 |
| PD | 5 | 7.7 | 6 | 9.2 |

D, docetaxel; DG, docetaxel plus gemcitabine; ECOG PS, Eastern Cooperative Oncology Group performance status; CR, complete response; PR, partial response; SD, stable disease; PD, progressive disease.

gemcitabine, respectively. Sixteen patients treated with docetaxel (25.0%) and 11 patients with docetaxel plus gemcitabine (16.9%) developed febrile neutropenia. All required antibiotic treatment and G-CSF; however, no patient died. One patient in the docetaxel plus gemcitabine arm developed anaphylatic shock immediately after administration of docetaxel at the second cycle. Grades 2–4 ALT elevation was more frequent with docetaxel plus gemcitabine than with docetaxel (20.0% versus 4.7%). Grades 2–4 non-neutropenic infection occurred more often with docetaxel plus gemcitabine than with docetaxel (21.5% versus 15.6%). Grades 2–4 ILD was more frequent with docetaxel plus gemcitabine than with docetaxel (16.9% versus 1.6%). Other toxic effects were relatively mild (Table 2). Overall, docetaxel plus gemcitabine was more toxic than docetaxel, however, well tolerated except for ILD in docetaxel plus gemcitabine arm.

## treatment efficacy

The overall response rate for docetaxel alone was 6.8% [95% confidence interval (CI) 1.9% to 16.5%] and 7.0% for docetaxel plus gemcitabine (95% CI 2.0% to 17.0%). There was no significant difference between treatment arms ($P = 0.71$; Fisher's exact test).

At the time of this analysis, 50 docetaxel patients (76.9%) and 48 docetaxel plus gemcitabine patients (73.8%) had died. The median survival time was 10.1 months for docetaxel alone and 10.3 months for docetaxel plus gemcitabine (one-sided $P = 0.36$ stratified log-rank test; Figure 2A). The respective 1-year survival rate was 43.1% (95% CI 31.0% to 55.1%) for docetaxel and 46.0% (95% CI 33.8% to 58.1%) for docetaxel plus gemcitabine.

The median PFS time was 2.1 and 2.8 months for docetaxel and docetaxel plus gemcitabine, respectively (one-sided $P = 0.028$ stratified log-rank test; Figure 2B).

**Table 2.** Hematological and non-hematological toxicity

| | D arm ($n = 64$) | | | | | DG arm ($n = 65$) | | | | |
|---|---|---|---|---|---|---|---|---|---|---|
| | NCI-CTC grade | | | | | NCI-CTC grade | | | | |
| Hematological | 0–1 | 2 | 3 | 4 | 3–4% | 0–1 | 2 | 3 | 4 | 3–4% |
| Anemia | 27 | 35 | 2 | 0 | 3.1 | 21 | 32 | 9 | 3 | 18.5 |
| Leukopenia | 9 | 14 | 29 | 12 | 64.1 | 11 | 12 | 32 | 10 | 64.6 |
| Neutropenia | 7 | 2 | 15 | 40 | 85.9 | 8 | 4 | 19 | 34 | 81.5 |
| Thrombocytopenia | 64 | 0 | 0 | 0 | 0 | 43 | 14 | 8 | 0 | 12.3 |
| Non-hematological | 0–1 | 2 | 3 | 4 | 2–4% | 0–1 | 2 | 3 | 4 | 2–4% |
| Allergic reaction | 64 | 0 | 0 | 0 | 0 | 59 | 5 | 1 | 0 | 9.2 |
| Alopecia | 45 | 18 | – | – | 28.1 | 49 | 14 | – | – | 21.5 |
| ALT | 61 | 2 | 1 | 0 | 4.7 | 52 | 10 | 3 | 0 | 20.0 |
| Diarrhea | 61 | 3 | 0 | 0 | 4.7 | 60 | 3 | 2 | 0 | 7.7 |
| Edema | 63 | 1 | 0 | 0 | 1.6 | 64 | 1 | 0 | 0 | 1.5 |
| Fatigue | 56 | 5 | 2 | 1 | 12.5 | 56 | 7 | 1 | 1 | 13.8 |
| Febrile neutropenia | 48 | – | 16 | 0 | 25.0 | 54 | – | 11 | 0 | 16.9 |
| Infection with grades 3–4 neutropenia | 59 | – | 5 | 0 | 7.8 | 56 | – | 9 | 0 | 13.8 |
| Infection without neutropenia | 54 | 8 | 2 | 0 | 15.6 | 51 | 4 | 9 | 1 | 21.5 |
| Nausea | 55 | 7 | 2 | – | 14.1 | 55 | 6 | 4 | – | 15.4 |
| Neuropathy | 62 | 2 | 0 | 0 | 3.1 | 62 | 2 | 0 | 1 | 4.6 |
| Pneumonitis (ILD) | 63 | 1 | 0 | 0 | 1.6 | 54 | 3 | 7 | 1 | 16.9 |
| Stomatitis | 61 | 3 | 0 | 0 | 4.7 | 60 | 5 | 0 | 0 | 7.7 |

D, docetaxel; DG, docetaxel plus gemcitabine; NCI-CTC, National Cancer Institute—Cancer Common Toxicity Criteria; ALT, alanine aminotransferase; ILD, interstitial lung disease.

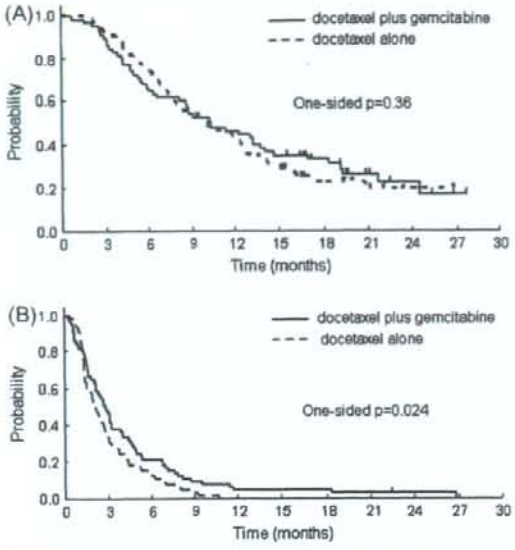


**Figure 2.** Overall survival (A) and progression-free survival (B) by treatment arm.

### disease-related symptom assessment

Patients' compliance with disease-related symptom assessment was 100% at baseline and 95.4% at 6 weeks later. Compliance rates were not different between the arms ($P = 1.00$). LCS data were missing in four surveys due to death or severe impairment of the patient's general condition; this accounted for 1.5% of the total number of surveys scheduled. Mean LCS at baseline and 6 weeks were shown in Table 3. There were no significant differences in the LCS changes from baseline to 6 weeks between docetaxel and docetaxel plus gemcitabine arms ($P = 0.61$).

## discussion

This trial was terminated early due to the unexpected high incidence of ILD and three treatment-related deaths due to ILD in the docetaxel plus gemcitabine arm. Our findings seem to indicate that the combination of docetaxel and gemcitabine may be associated with a higher incidence of pulmonary adverse events compared with docetaxel alone, especially in patients with previously treated NSCLC.

Pulmonary toxicity following chemotherapeutic agents, including ILD, has been well recognized for many years. In most cases, this toxicity is mild and self-limiting. However, the mechanism of developing drug-induced ILD is uncertain, and risk factors for developing this disorder have not been identified. In terms of combination therapy with docetaxel and gemcitabine for advanced NSCLC, there were few reports about the incidences of ILD at the time this study was planned. A phase I study of patients with transitional cell carcinoma evaluated thrice-weekly doses of docetaxel given on day 1 plus gemcitabine given on days 1 and 15 and showed that pulmonary toxicity occurred in three of five patients and was

**Table 3.** Disease-related symptom assessment

| Lung Cancer Subscale | D arm | DG arm |
|---|---|---|
| Baseline | | |
| Number | $n = 65$ | $n = 65$ |
| Mean ± SD | 19.0 ± 5.48 | 19.7 ± 5.25 |
| 6 weeks later | | |
| Number | $n = 62$ | $n = 62$ |
| Mean ± SD | 18.1 ± 5.56 | 18.9 ± 5.05 |
| Difference | | |
| Mean ± SD | −1.11 ± 3.81 | −0.99 ± 4.49 |

D, docetaxel; DG, docetaxel plus gemcitabine; SD, standard deviation.

the cause of death in one [25]. Recently, some reports have been published about the high incidence of ILD due to the combination regimen of docetaxel and gemcitabine in patients with NSCLC [13, 26, 27], including the present study (Table 4). In Japanese population, ILD is a very complex issue in treatment of patients with lung cancer. Epidermal growth factor tyrosine kinase inhibitor gefitinib is developing ILD significantly in Japanese patients with NSCLC [28]. It is uncertain why ILD is developing more in Japanese patients with NSCLC than the Western patients. Ethnic difference may be one of the explanations for this occurrence. The combination of gemcitabine and docetaxel is associated with a high incidence of severe pulmonary toxicity. The regimen should not be used outside a clinical trial.

The median survival times of 10.1 and 10.3 months and estimated 1-year survival rates of 43.1% and 46.0% with docetaxel alone and docetaxel plus gemcitabine, respectively, suggest that adding gemcitabine to docetaxel did not provide any increased efficacy in patients with previously treated NSCLC. Interestingly, the combination regimen of docetaxel plus gemcitabine significantly improved the median PFS time ($P = 0.028$). Possible reasons for failing to detect a significant difference between survival curves may include an insufficient occurrence of documented events as a result of the study population comprising patients with relatively good prognosis, in addition to a high proportion of patients subsequently receiving third-line therapy. During this study, gefitinib treatment was commonly used for patients with recurrent NSCLC in Japan [29]. Asian ethnicity is a well-known predictive factor for a response for gefitinib [30].

Two randomized phase II trials compared docetaxel alone with docetaxel plus irinotecan in second-line chemotherapy for NSCLC [31, 32]. No significant treatment differences in survival were observed in either trial; however, the trials were phase II study and were not powered or designed to compare survival. This study was not powered to compare survival when it was terminated early due to the unexpected high incidence of ILD in the docetaxel plus gemcitabine arm. However, based on previous studies, as well as the present results, combination chemotherapy with docetaxel and another chemotherapeutic agent has not improved survival in patients with previously treated NSCLC.

In conclusion, docetaxel alone is still the standard second-line treatment for advanced NSCLC. The combination of docetaxel and gemcitabine was too toxic to obtain any survival